Sensitivity and Uncertainty Quantification of Continuum and Stochastic Bond Dissociation Kinetics Based Cohesive Laws

By

Rishabh Awasthi

A REPORT

Submitted in partial fulfillment of the requirements for the degree of

MASTER OF SCIENCE

In Degree Program

MICHIGAN TECHNOLOGICAL UNIVERSITY

2020

Table of Contents

List of figures 3

List of tables 6

Acknowledgements 7

Abstract 8

1 Sensitivity Analysis & A Machine Learning Approach for Inverse Calibration of a rate dependent Cohesive Zone Model 9

1.1 Abstract 9

1.2 Introduction 9

1.3 Background: Experiment and Theory 11

1.3.1 Mode I Fracture: Double Cantilever Beam Experiment 11

1.3.2 Rate Dependent Cohesive Zone Model 13

1.3.3 Numerical Simulation: 14

1.4 Inverse Calibration based on Uncertainty Quantification 17

1.4.1 Sensitivity Analysis: Sobol Indices 17

1.4.2 Training Data 18

1.4.3 K Nearest Neighbor Regression 19

1.4.3.1 KNN Regression Results, Model Output: Fracture Energy (Gf) 20

1.4.3.2 KNN Regression Results ,Model Output: Maximum Force (Fmax) 22

1.4.3.3 KNN Regression Results, Model Output: Fracture Energy (Gf) 23

1.4.3.4 KNN Regression Result 25

1.5 Model Verification: 25

1.6 Model Validation: 26

2 Stochastic bond dissociation kinetics approach for a rate dependent Cohesive Zone Model 27

2.1 Abstract 27

2.2 Background: Theory 27

2.3 Stochastic Bonding Cohesive Law: Polymeric Adhesive 30

2.3.1 Calculation for Cohesive Law, Quasi-Static Strain Rate:5.08 mm/ min 30

2.3.2 Results: Quasi-Static (Strain Rate: 5.08 mm/min) 31

2.3.3 Stochastic Bonding Cohesive Law Estimation for Higher Strain Rates 33

2.4 Results 35

3 Material calibration and Cohesive Zone Modelling approach to predict Interfacial Adhesion of Mussel Inspired Smart Adhesives 37

3.1 Abstract 37

3.2 Introduction 37

3.3 Experimental Results:....38
3.3.1 Contact Mechanics Test:....38
3.3.2 Experimental Results: Force vs Displacement Plot....39

3.4 Numerical Simulation: Contact Mechanics Test....39
3.4.1 Simulation Setup Abaqus....41

3.5 Material Calibration 43
3.5.1 Hyperelastic Material Model 43
3.5.2 Viscoelasticity....45
3.5.3 Material Calibration Results: 47

3.6 CZM parameters Calibration....48
3.6.1 Cohesive zone modelling....48
3.6.2 CZM parameter calibration....50

Sensitivity Analysis 52

3.7 Results & Discussion....53

3.8 Acknowledgement....54

4 Summary....55

5 Reference List 56

List of figures

Figure 1.1 : Schematic of Experimental setup for a DCB Specimen.....12

Figure 1.2 : Experimental Force vs Displacement Curve for three strain rates : 5.08mm/min , 50.8 mm/min , 508 mm/min.....12

Figure 1.3 : A general representation of a traction separation curve for a polymeric adhesive.....14

Figure 1.4 : Schematic Representation of Crack Opening Mechanism for a Rigid Cantilever Beam (RDCB) Specimen 15

Figure 1.5 : Traction Separation Laws Assumed for Strain Rates : 5.08 mm/min , 50.8mm/min , 508 mm/min to perform Numerical Simulation.....16

Figure 1.6 : Force vs COD Plot to compare the Numerical Simulation with the Experimental response at Strain Rate : 5.08 mm/min.....16

Figure 1.7 : Sobol Indices of Order 1 18

Figure 1.8 : Force vs COD plots N=10000 Training Samples generated by Latin Hypercube Sampling.....19

Figure 1.9 : Model Response : Fracture Energy(Gf) for N=10000 Training Samples 20

Figure 1.10 : Comparison of model prediction with the experiment for the F vs COD curve 21

Figure 1.11 : Model Response : Fracture Energy(Fmax) for N=10000 Training Samples 22

Figure 1.12 : Comparison of model prediction with the experiment for the F vs COD curve 23

Figure 1.13 : Model Response : Force at COD =20 (Fopen) for N=10000 Training Samples.....23

Figure 1.14 : Comparison of model prediction with the experiment for the F vs COD curve 24

Figure 1.15 : Comparison of F vs COD curve between Predicted Model and Experiment 25

Figure 1.16 : Comparison of F vs COD curve between Predicted Model and Experiment for Strain Rate : 50.08 mm/min , Prediction Error % = 2.2924.....26

Figure 1.17 : Comparison of F vs COD curve between Predicted Model and Experiment for Strain Rate : 50.08 mm/min , Prediction Error % = 1.6439 26

Figure 2.1 : Single Spring Bond Complex 28

Figure 2.2 : Bond Potential Energy as function of interatomic distances 28

Figure 2.3 : Evolution of bonding probability at different Strain Rates (nm/sec) 29

Figure 2.4 : Stochastic Traction Separation Law at different Strain Rates (nm/sec) 29

Figure 2.5 : Comparison of Stochastic-Bonding and Phenomenological (Viscoplastic Flow Rule) based Traction Separation Law for Strain Rate : 5.08mm/min 31

Figure 2.6 : Evolution of bonding probability as function of separation for a strain rate : 5.08 mm/min 32

Figure 2.7 : Prediction of Stochastic-Bonding and Phenomenological (Viscoplastic Flow Rule) based Cohesive Laws for Mode-I Fracture , Strain Rate : 5.08 mm/min 32

Figure 2.8 : Comparison of Stochastic-Bonding and Phenomenological (Viscoplastic Flow Rule) based Traction Separation Law for Strain Rate : 50.8mm/min 33

Figure 2.9 : Prediction of Stochastic-Bonding and Phenomenological (Viscoplastic Flow Rule) based Cohesive Laws for Mode-I Fracture , Strain Rate : 50.08 mm/min .. 34

Figure 2.10 : Comparison of Stochastic-Bonding and Phenomenological (Viscoplastic Flow Rule) based Traction Separation Law for Strain Rate : 508mm/min 34

Figure 2.11 : Prediction of Stochastic-Bonding and Phenomenological (Viscoplastic Flow Rule) based Cohesive Laws for Mode-I Fracture , Strain Rate : 508 mm/min 35

Figure 2.12 : Stochastic Bonding : Predicted Mode-I Fracture Response for 3 strain rates 36

Figure 3.1 : Schematic of Contact Mechanics Experiment Conducted to characterize interfacial binding property of adhesive hydrogel 38

Figure 3.2 : Force vs Displacement Plot : Adhesive (D10B10) 39

Figure 3.3 : Schematic Diagram for Inverse Calibration of Material Response of Adhesive Hydrogel conducted in Abaqus Implicit 40

Figure 3.4 : Mesh Generated with linear axisymmetric elements: CAX3H , CAX4RH ... 41

Figure 3.5 : Part Assembly with Boundary Conditions 42

Figure 3.6 : Contour : Max in-plane principal logarithmic strain.....42

Figure 3.7 : Arruda Boyce material model calibration results for different iterations 44

Figure 3.8 : Maxwell and Weichert Model.....45

Figure 3.9 : Stress Relaxation Experiment 46

Figure 3.10 : Comparison of viscoelastic response with experiments considering the number of maxwell elements (no. of terms in prony series).....46

Figure 3.11 : Stress Relaxation comparison between number of maxwell elements.....47

Figure 3.12 : Simulation prediction based on material parameters in Table 3.2,3.3 48

Figure 3.13 : Diagrams to depict failure modes [37].....48

Figure 3.14 : Interfacial failure of polymeric adhesive.....49

Figure 3.15 : Pure Mode I,II,III Bilinear Traction Separation Law.....49

Figure 3.16 : Damage Progression of Adhesive, Red contour indicates complete debonding of adhesive from substrate 51

Figure 3.17 : Comparison of adhesive strength predicted by cohesive law with the experiments.....51

Figure 3.18 : Tornado diagram for sensitivity analysis 53

Figure 3.19 : Results of Contact Mechanics Numerical Simulation.....53

List of tables

Table 1.1 : Values of Input Parameters of Traction Separation Law giving a good match the experimental results 15

Table 1.2 : $\theta Gf*$: Predicted Input Parameters by KNN Regression based on Model Response : Facture Energy (Gf).....21

Table 1.3 : $\theta Fmax*$: Predicted Input Parameters by KNN Regression based on Model Response : Maximum Force (Gf) 22

Table 1.4 : $\theta Fopen*$: Predicted Input Parameters by KNN Regression based on Model Response : Force at COD=20 mm (Fopen) 24

Table 1.5 : Predicted Input Values of Traction Separation Law for KNN Regression 25

Table 2.1 : Parameters governing the stochastic bonding based rate dependent traction separation law 30

Table 2.2 : Parameters stochastic bonding based rate dependent traction separation law for a strain rate : 5.08 mm/min.....31

Table 2.3 : Percentage Error for 3 strain rates 35

Table 3.1 : Arruda Boyce material parameters to perform inverse calibration. 44

Table 3.2 : Hyperelastic material parameters 47

Table 3.3 : Viscoelastic material parameters 47

Table 3.4 : Input Parameters governing the surface based traction separation law.....50

Acknowledgements

I would like to express my sincere gratitude to my advisor Dr Trisha Sain for the continuous support of my masters study and research, for her patience, motivation, enthusiasm, and immense knowledge. Her constant guidance and support helped me stay focused on my research tasks and motivated me to work with passion and dedication. Further , I would like to thank my graduate research committee Dr. Gregory Odegard , Dr. Bruce P Lee and Dr. Trisha Sain for being an integral part of my masters report defense. I really appreciate the deep insight and review points shared with me during my oral presentation. I wish to acknowledge the support given by Dr. Muhammad Imam and Dr. Ameya Narkar by sharing their research work which I used as basis to conduct my research. I wish to thank my parents and my sister for their unconditional love and constant motivation to follow my dream of pursuing a master's degree in mechanical engineering. It has been a long journey full of ups and downs in which my family has always a solid rock of support and encouragement which helped push through the challenging times.

Abstract

Polymeric adhesives are being extensively used to develop light weight and durable Composite Materials which are have been employed in automotive, aeronautical, medical industry. Polymeric adhesives undergo failure due to relative opening sliding of bonded interfaces which requires a need to characterize the fracture mechanism. Numerous experiments are conducted to predict the fracture response for Mode-I, II,III and numerical simulations are employed to inversely calibrate the material parameters governing the constitutive laws. Cohesive zone models are largely employed in fracture mechanics to predict failure of interfaces undergoing large plastic deformations. The objective of this report is to employ the cohesive zone models to predict fracture of polymeric interfaces. Cohesive zone models are governed by traction separation relationships which can be defined both at the continuum level which is macroscale and at the molecular/atomic level. The report is organized into three sections: 1st section is focused on a machine learning approach to characterize the rate dependent response of polymeric adhesive by inverse calibration of a continuum based cohesive zone parameters. The 2nd section aims to develop a stochastic bond kinetics based cohesive law defined at microscopic level to predict the rate dependent fracture. The 3rd section's objective is to perform material and cohesive zone calibration to characterize the adhesive strength of smart adhesives.

1 Sensitivity Analysis & A Machine Learning Approach for Inverse Calibration of a rate dependent Cohesive Zone Model

1.1 Abstract

Polymeric adhesives employed in developing composites have demonstrated a rate dependent fracture response which significantly affects the interfacial failure mechanisms. An elastic-viscoplastic cohesive zone model to predict Fracture in Mode I, II at different strain rates by considering a polymer viscoplastic flow rule defined for normal opening and tangential sliding along the interface.[1] The present framework was implemented in a Numerical Simulation in an Explicit Time Scheme to quantify Mode-I Fracture in a Rigid Double Cantilever Beam (RDCB) Experimental Setup under the assumption of Material Stiffness of Beam being high as compared to the Adhesive[2].The zero thickness cohesive surface interactions which are governed by the traction separation relationships are employed in computational model to predict the damage at the interface[3].The model requires a set of N input parameters to define the traction separation law which are mostly non-deterministic in nature since they can't be measured experimentally nor controlled by the user. The aim of this study is to develop a methodology based on a K-Nearest Neighbor Regression Algorithm to predict the input model parameters by inverse calibration based on the experimental results at different strain rates.

1.2 Introduction

Composite Materials have a combination mechanical property of two or more materials which provides immense design flexibility for developing Light Weight Structures with a High Stiffness to Weight Ratio, Fatigue and Corrosion Resistance. Composite Structures have found widespread application in Automobile, Packaging, Medical and Marine Industry owing to numerous advantages mentioned[4].Polymeric Adhesives are categorized as Thermosetting (polyurethanes) and Thermoplastics (epoxies)[5] have been extensively used for bonding Layers of Dissimilar Materials present in Laminate Composites. Polymeric Adhesives replace the traditional methods of fastening such as bolts and rivets which reduced the structural integrity of composites due to stress concentration which tend to be the root cause of Structural Fatigue owing to Dynamic loading. Adhesives are applied on large surface area which ensure even distribution of load increasing fracture resistance and are corrosion resistant to highly reactive chemicals[6].The widespread application of Laminate Composites for Highly Dynamic Loading Scenarios encountered by automobiles, aircrafts and carriers during their service cycle has prompted research to study interfacial failures and delamination of polymeric adhesives.

The bonding interface of the adhesive with the substrates plays a significant role to determine the fracture Energy of the adhesives since the crack initiation and propagation

occurs due to relative motion of the contact surfaces at the interface in normal (Mode-I) and shear directions (Mode II, III)[7]. Polymer based adhesives have demonstrated rate dependent mechanical response and a study indicates a relationship between polymer chain entanglement and viscoelasticity[8].Further, numerous experimental studies have observed a significant effect on fracture properties of bonded interfaces due to change in strain rates [9], [10]. Therefore, it is very important to develop an interfacial constitutive model which can accurately predict the interfacial failure at different strain rates.

Fracture Testing Standards such as Double Cantilever Beam (DCB) and End Notched Flexure (ENF) are employed to experimentally measure the Fracture Energy (Gc) in pure Mode I and Mode II respectively by calculating the area under Force Displacement curve. ENF test configuration has been modified by adding a roller at joint interface which induces mixed mode behavior and is employed to measure Fracture Energy in mixed mode Mode I,II [11]. These methods are designed to characterize fracture for quasi-static loading but are not suitable to predict fracture for high strain rates (impact loading) due to discrepancy in experimental measurements. A Split Hopkinson Bar method can accurately capture stress – strain response for high strain rates for soft materials such as polymers [12].

Cohesive zone models have been widely implemented in numerical simulations to predict fracture in metallic, polymeric, ceramic materials and their composites[13]. The model assumes the complex microscopic failure process at the bonded interface with a nonlinear fracture process zone which is defined by cohesive surface interactions or cohesive elements [3]. Traction separation relationships are defined in the cohesive zone models to predict the failure properties (fracture toughness, cohesive strength and maximum opening) in mode-I, II and mixed mode fracture [10]. Traction separation curves can be developed by conducting fracture experiments such as double cantilever beam test through direct and inverse techniques which typically assume a bilinear relationship of the curve. J-integral contours are evaluated to directly measure the cohesive response which poses a disadvantage in terms of experiment capability[14]. The inverse method employs finite element model to predict the cohesive zone parameters to best match the experimental force vs displacement curve.

A modification has been proposed to the double cantilever fracture test which considers the stiffness of the substrate being higher as compared to the polymeric adhesive . This underlying assumption is employed to develop an analytical solution of the traction separation law based on the experimental force vs crack opening displacement curve for mode-I failure. Cohesive zone models have been developed to incorporate the viscoelastic material response of polymers and adhesive joints under the assumption of rate dependency arising due to dissipation at the interfaces [15]. The phenomenological surface based interfacial model developed by characterizes the rate dependency of adhesives by considering visco-plastic flow rule for glassy polymers [16]. This rate dependent cohesive law was implemented in an explicit – numerical time scheme in MATLAB to calculate a force vs COD response of adhesives in a rigid double cantilever beam experiment to characterize mode-I fracture. Further, the numerical implementation was validated with

experiments conducted to study the rate dependent fracture response on high density-polyethylene based adhesives [17].

The rate dependent cohesive zone model is mathematically represented as Ym = f(x,θ) in which Ym represents the model response and x,θ represents the model parameters. x = [x1, x2, x3….] represents the model parameters which are deterministic in nature in since they can be measured while conducting the experiment. The present model has strain Rate, crack Length, dimensions of the beam as deterministic model parameters. $\theta = [\theta 1, \theta 2, \theta 3 \ldots]$ model parameters are non-deterministic in nature since they are unknown over the course of the experiment. The traction separation law is governed by a set of 7 parameters are non-deterministic and require calibration to accurately match the experimental results. The first step to calibrate input model parameters (θ) is to assume each parameter as a random variable following a probability distribution function (pdf) (Normal, Log-Normal). This probabilistic nature of the input parameter is the source of uncertainty in the model output which requires an uncertainty quantification. This method has been extensively used for predictive modelling of engineering design scenarios to characterize and investigate the input parameters governing the mathematical model[18]. A sensitivity analysis is conducted to determine the impact in variance of model response due to variance of each input parameter (θ). This methodology aids in identification of non-critical input parameters and is an effective method for dimensionality reduction of the assumed random input space. Random sampling techniques such as monte carlo simulations (MCS) and latin hypercube sampling (LHS) are employed to generate N samples of training data. The training data is generated for a quasi-static loading with a strain rate of 5.08 mm/min. The objective is estimate is to develop a model which accurately predicts the experimental response for quasi-static loading. This trained model will be validated for higher strain rates to account rate dependency. This K nearest neighbor Regression is a supervised machine learning algorithm which identifies K nearest input samples based on the close proximity of model response with experimental response. The training data is employed to train the mathematical model based on a K – nearest neighbor regression algorithm to predict the calibrated input parameters (θ *). The calibrated parameters are used to predict model response at Higher Strain Rates (50.8 mm/min and 508 mm/min) and compared with experimental response for Model Verification.

1.3 Background: Experiment and Theory

1.3.1 Mode I Fracture: Double Cantilever Beam Experiment

Double cantilever beam (DCB) test was conducted to predict rate dependent Mode–I fracture toughness of high-density-polyethylene based thermoplastic adhesive. The DCB specimen is composed of an aluminium alloy(Al 6061-T6) as substrate with 0.2mm thickness of adhesive bond with an initial crack length 101.60mm. The DCB experiment were conducted for three strain different rates: 5.08, 50.8, 508 mm/min and a tensile force vs crack opening displacement (F vs COD) curves were plotted. The Fracture Energy (Gf)

is calculated as the area under the F vs COD curve ($\int Fdx$) which increased for Higher Strain Rates. [19]

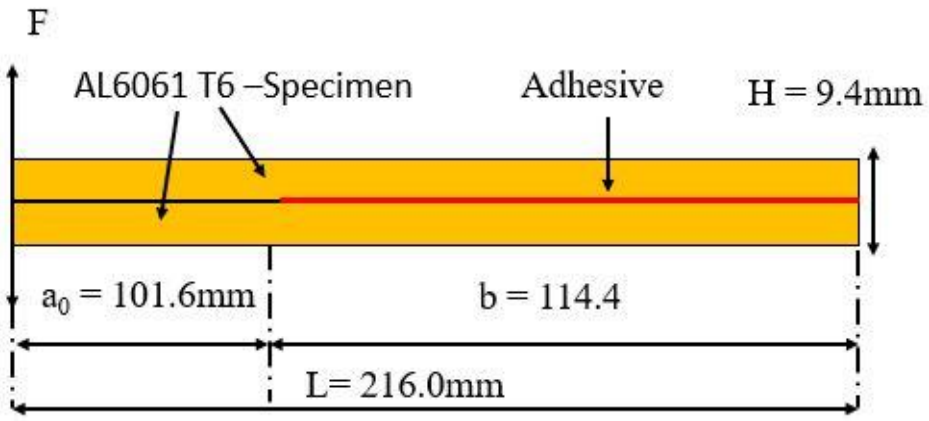

Figure 1.1 : Schematic of Experimental setup for a DCB Specimen

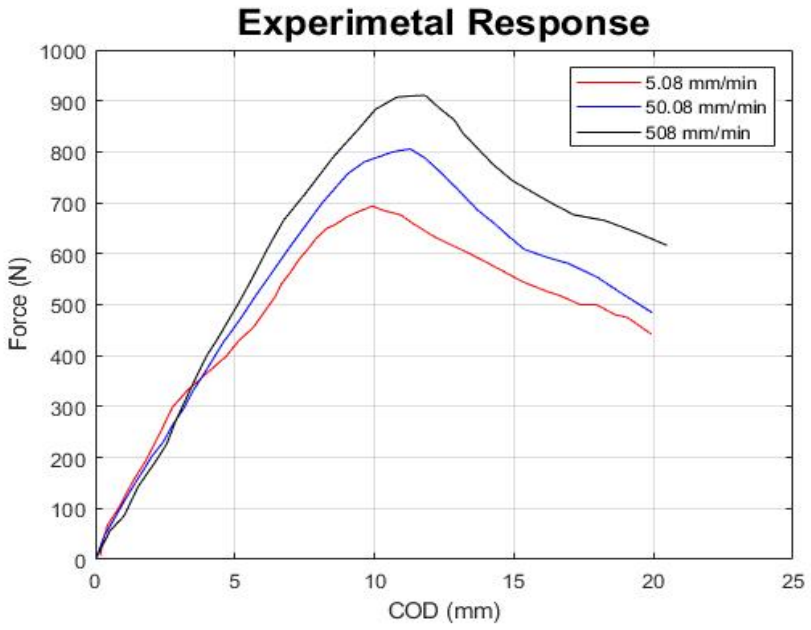

Figure 1.2 : Experimental Force vs Displacement Curve for three strain rates : 5.08mm/min , 50.8 mm/min , 508 mm/min

1.3.2 Rate Dependent Cohesive Zone Model

The general expression of rate independent traction separation law governing the interfacial failure for pure mode-I fracture:

$$T(\delta) = \begin{pmatrix} K_n\delta \ , \ 0 < \delta < \delta i \\ (1-D)K_n\delta \ , \delta_i < \delta < \delta_f \end{pmatrix} \quad 1$$

$$D = \frac{\delta(\delta_f - \delta_i \ )}{\delta_f(\delta - \delta i)}, \delta_i < \delta < \delta_f \quad 2$$

$T \ , K_n \ , \delta, \delta_i \ , \delta_f \ , D$ represent Surface Traction, Normal Stiffness, Normal Separation between the interface, Normal Separation at Damage Initiation, Normal Separation at Complete Failure & Scalar Damage Variable which evolves from 1 to 0 during the fracture process. The area under Traction Separation Curve ($\int T d\delta$) is the Fracture Toughness of the material.

The experiments conducted on high density polyethylene based on thermoplastic adhesive indicated difference in Mode-I Fracture response at various strain rates which can characterized by a strain rate dependent traction separation law[20]. This constitutive law defines the surface traction of the adhesive interface as a function of the separation between them. The separation is caused due to elastic and plastic deformations at the interface due to crack opening and sliding under external loading causing Adhesive Failures in Mode I, II, III. This constitutive law is extended to a large deformation framework to account for finite displacements of polymers and a visco-plastic flow rule based on thermally activated motions of dislocation is employed to incorporate strain rate dependency for plastic deformation. This flow rule based on [21] , [22]calculates the inelastic deformation rate based on the following Equation:

$$\nu^i = \nu_o \exp\left(-\frac{Q}{k\theta}\right)\left[\sinh\left(\frac{t^e_{N,t}V}{2k\theta}\right)\right]^{\frac{1}{m}} \quad 3$$

$t^e_{N,t} \ , \nu \ , Q \ , k \ , \theta, V \ , m$ represent the net stress for thermally activated flow, the pre-exponential factor, the activation energy, the Boltzmann's constant, the absolute temperature, the activation volume and the rate sensitivity parameter respectively. This interfacial constitutive model can be implemented for an Explicit Numerical Time Scheme in commercial finite element packages to predict Force vs Displacement curves for fracture experiments conducted for Pure Mode I,II and Mixed Mode Failures. The Numerical Simulation can be simplified under the assumption that the stiffness of the Beam is very high as compared to the adhesive which will be discussed in detail in the next section.

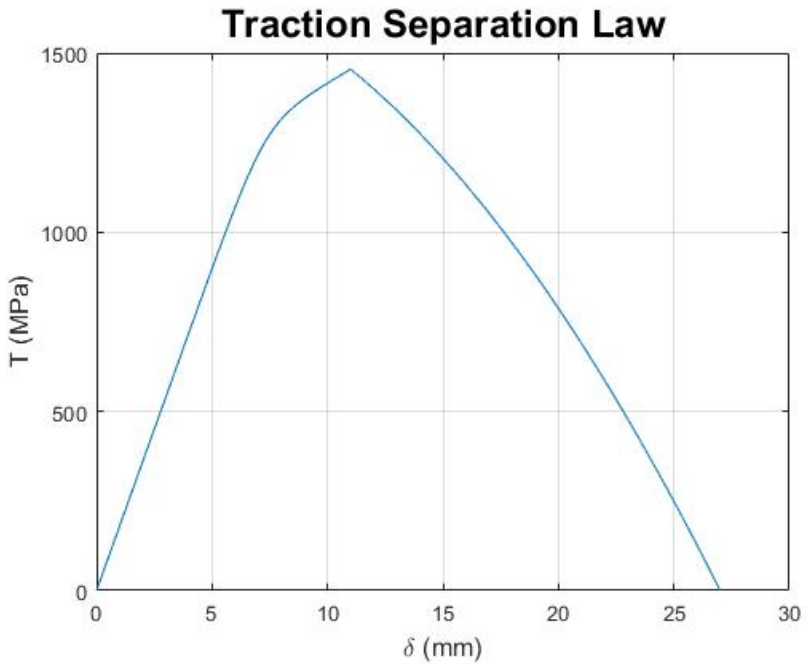

Figure 1.3 : A general representation of a traction separation curve for a polymeric adhesive

1.3.3 Numerical Simulation:

The rate dependent Traction Separation Law developed using Eq [1,2,3] was implemented in a Numerical Simulation of a Double Cantilever Beam Experiment conducted earlier to predict the Force vs COD Curve which was verified by quantifying the error by comparing it with the Experimental Response. The simulation framework developed is based on an underlying assumption of Cantilever Beam has high material stiffness as compared to the adhesive which ensures that the strain energy released the during the crack propagation is stored in the adhesive itself.[2] This setup is termed as Rigid Cantilever Beam(RDCB) Specimen defines a relationship between Crack Opening Displacement (COD) and the Separation (δ) at a given spatial point x and time 't' which is defined as

$$\delta(x,t) = \left(\frac{x}{L}\right) COD(t) \qquad 4$$

where $\delta(x,t), L, COD$ represent separation at spatial point "x" along length of the Beam and time 't', Length of the Beam, Crack Opening Displacement. Further the Moment Balance Equation developed an Analytical Correlation between the Traction Separation Law with the Force vs COD curve governed by the following Equation:

$$B \int_0^b xt(x,t) = LF(t) \quad 5$$

where $B, t(x,t), L, F(t), b$ represents the width of the beam, traction at spatial point 'x' and time 't', length of the beam, Tensile Force at time 't' and length of adhesive bond respectively

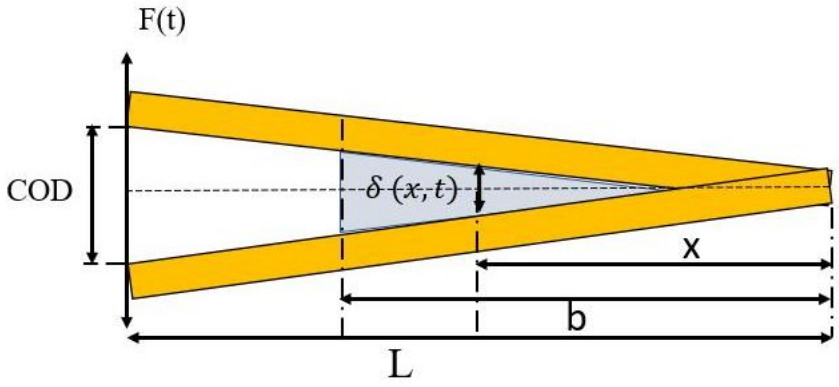

Figure 1.4 : Schematic Representation of Crack Opening Mechanism for a Rigid Cantilever Beam (RDCB) Specimen

This simulation framework was implemented in MATLAB for a strain rate of 5.08 mm/min which is assumed to be quasi-Static which calculates force vs crack opening displacement (COD) curve for a set of traction separation parameters. The given set of parameters are verified by comparing with experimental force vs COD curve for the same strain rate. Further the model was validated for High Strain Rates of 50.8 mm/min and 508 mm/min by updating the strain rate keeping input parameter governing the traction separation law as same. The given set of input parameters governing the traction separation law gave a good match to the experimental response : force vs COD curve. The given parameters drive the phenomenological rate dependent cohesive law which gives model response as force vs COD curve when implemented in DCB numerical simulation.

K_n (MPa/mm)	S_o (MPa)	δ_i (mm)	$\delta_f(mm)$	H (MPa/mm)	v_o(mm/s)	Q(J)
170	260	10.5	27.0	10.0	1e-05	1e-20

Table 1.1 : Values of Input Parameters of Traction Separation Law giving a good match the experimental results

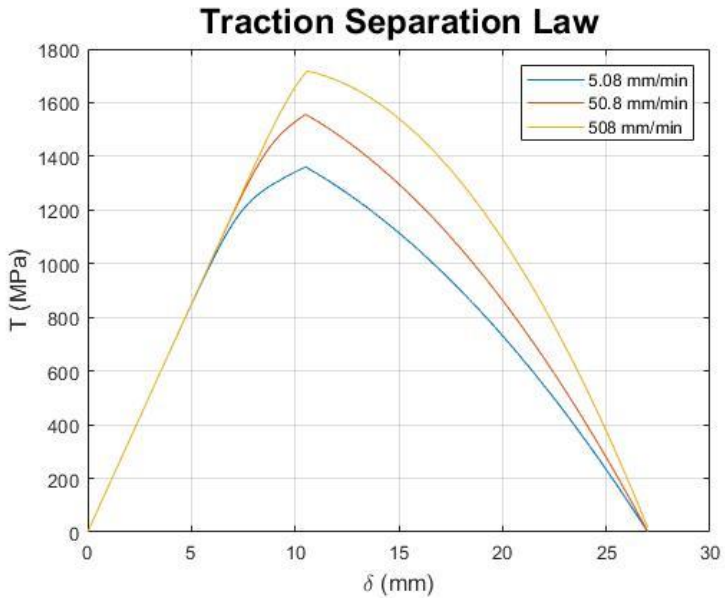

Figure 1.5 : Traction Separation Laws Assumed for Strain Rates : 5.08 mm/min , 50.8mm/min , 508 mm/min to perform Numerical Simulation

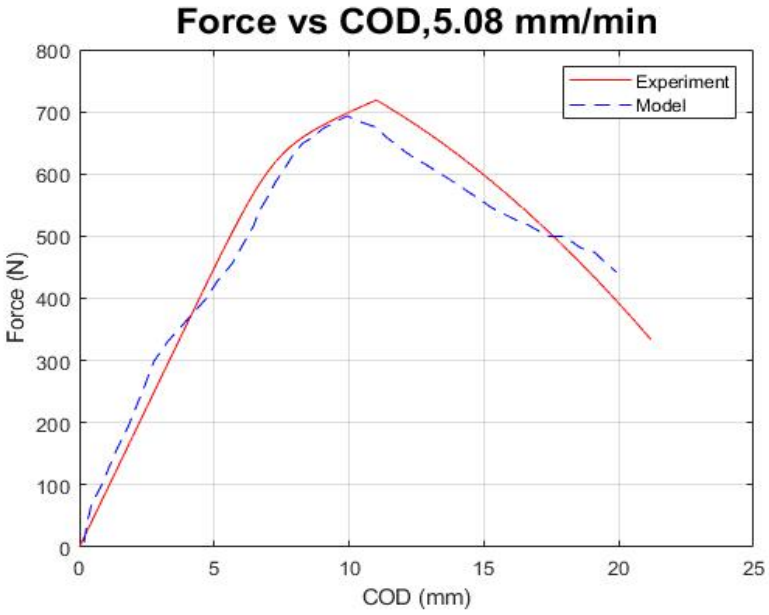

Figure 1.6 : Force vs COD Plot to compare the Numerical Simulation with the Experimental response at Strain Rate : 5.08 mm/min

1.4 Inverse Calibration based on Uncertainty Quantification

The Traction Separation Law is driven by 7 independent parameters introduce uncertainty into the computational model and require calibration to match with the experimental response. The following steps are followed for uncertainty analysis.

The Computational Model is represented as $Ym = f(X, \theta)$ where X: Deterministic parameters (crack length, strain rate) , θ : Non-deterministic parameters (Traction Separation Law) , Ym: model prediction , Ye: experimental response. We assume probability distribution function (Normal or Log Normal) for random variables θ and perform sensitivity analysis to identify critical parameters. Training data is generated based on latin hypercube sampling technique and KNN regression algorithm is employed to predict $\theta*$ which is closest to the experimental results. The computational model response is evaluated at $\theta*$ by comparing with experimental response for quasi-static loading. The trained model is validated by comparing model response with experiments at high strain rates.

1.4.1 Sensitivity Analysis: Sobol Indices

Sobol indices is a Variance based global sensitivity analysis which decomposes the variance of the model output into variance of each input parameter governing the mathematical model. The computational model is denoted as:

$$Ym = f(\theta_1, \theta_2 \dots \dots \dots \theta_n) \quad 6$$

Where Ym represents the model response: Fracture Energy and θ represent input variables governing the Traction Separation Law the This decomposition only holds for independent input variables. The first order Sobol Indices is given as: [23]

$$V(Y) = \sum_{i=1}^{n} Vi \quad 7$$

n represents the number of input parameters which are 7 in our case. To perform the sensitivity we first assumed that the each input parameter follows Normal Probability Distribution ($\theta \sim (\mu, \sigma^2)$) :

$$\mu = [170\ 260\ 10.5\ 27\ 10\ 1e-5\ 1e-20] \quad 8$$

$$\sigma^2 = [289\ 676\ 1.025\ 7.29\ 1\ 1e-12\ 1e-42] \quad 9$$

where μ represents the mean vector and σ^2 represents the variance vector. The mean vector μ is the cal

The Sensitivity Analysis was conducted in UQLAB to get the following result.

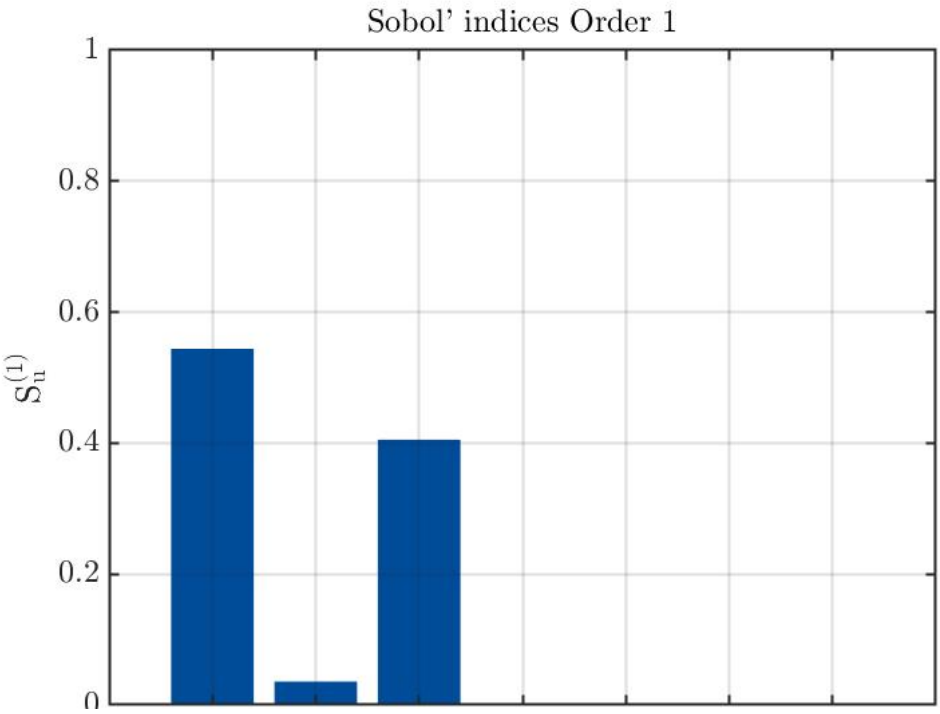

Figure 1.7 : Sobol Indices of Order 1

The results indicate that Kn , δ_i , δ_f are the important input parameters which affect the output Fracture Energy the most.

1.4.2 Training Data

The training data was generated by using Latin Hypercube Sampling Technique for 10000 Samples assuming a Normal Probability Distribution: $\theta \sim (\mu, \sigma^2)$ with values referred from Equation [8,9]. The model will be trained based on dataset generated for a Quasi-Static Simulation which has a strain rate of 5.08 mm/min. The trained model will be evaluated at Higher Strain Rates for validation. We decided to evaluate the model response (Ym) at 3 scalar outputs: Fracture Energy , Maximum Force , Force at COD=20 mm which was extracted from N samples by the model's prediction of the Force vs Displacement Curve. We chose 3 model responses to capture the non-linear Force vs COD curve for the experiment which will further aid in develop a more effective KNN Regression Algorithm

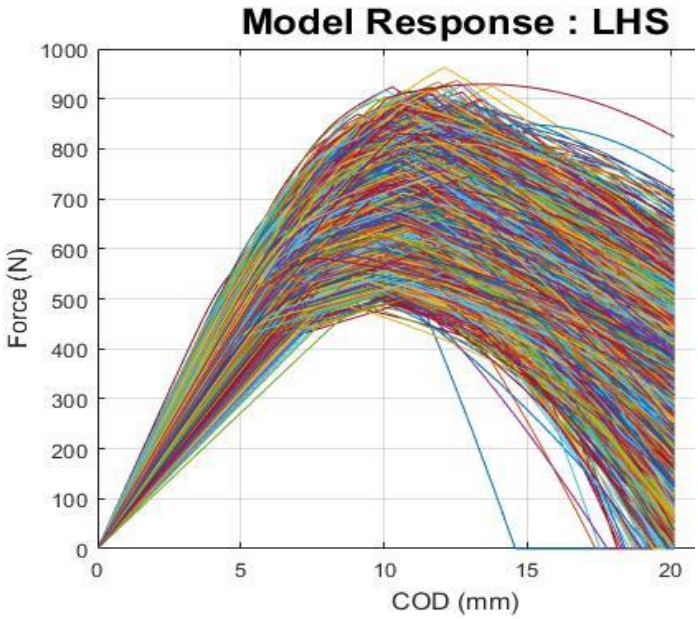

Figure 1.8 : Force vs COD plots N=10000 Training Samples generated by Latin Hypercube Sampling

1.4.3 K Nearest Neighbor Regression

K Nearest Neighbor is an efficient and easy to implement supervised machine learning algorithm[24]. The objective of this algorithm is to identify K nearest samples from the training dataset for which the model response chosen in earlier section is at proximity with the Experimental Response. This is achieved by calculating the Euclidean distance between the Model Response and the Experiment for each training sample and sorting distance in increasing order. We choose "K" closest Euclidean distances and extract the indexes of each sample if input parameter. The model prediction is the mean of the K input parameter. This predicted θ^* which is the calibrated input parameters for the traction separation law is then employed to Run the RDCB Numerical Simulation to predict the Force vs COD curve and compared with Experiments to compute the prediction error.

The KNN Regression Algorithm can be summarized as follows:

1. Training Data Set: $Yi_m = f(\theta i_1, \theta i_2 \ldots . \theta i_n)$, i = 1,2 … … N
2. Compute Distance : Di = $\sqrt{(Y_e - Yi_m)^2}$ (Euclidean Distance), Ye : Test Data
3. Identify "K" nearest Di and corresponding Input Data Set : $\theta = [\theta i1, \theta i2 \ldots . \theta in]$, $i = 1,2 \ldots . K$
4. Compute Mean to Calculate learned θ*: $\theta_j* = \frac{1}{K} \sum_{i=1}^{K} \theta_{ij}$, i = 1,2….. K , j = 1,2…….n)
5. Evaluate Model Response Ym* at θ* by comparing with Test Data to compute Error

1.4.3.1 KNN Regression Results, Model Output: Fracture Energy (Gf)

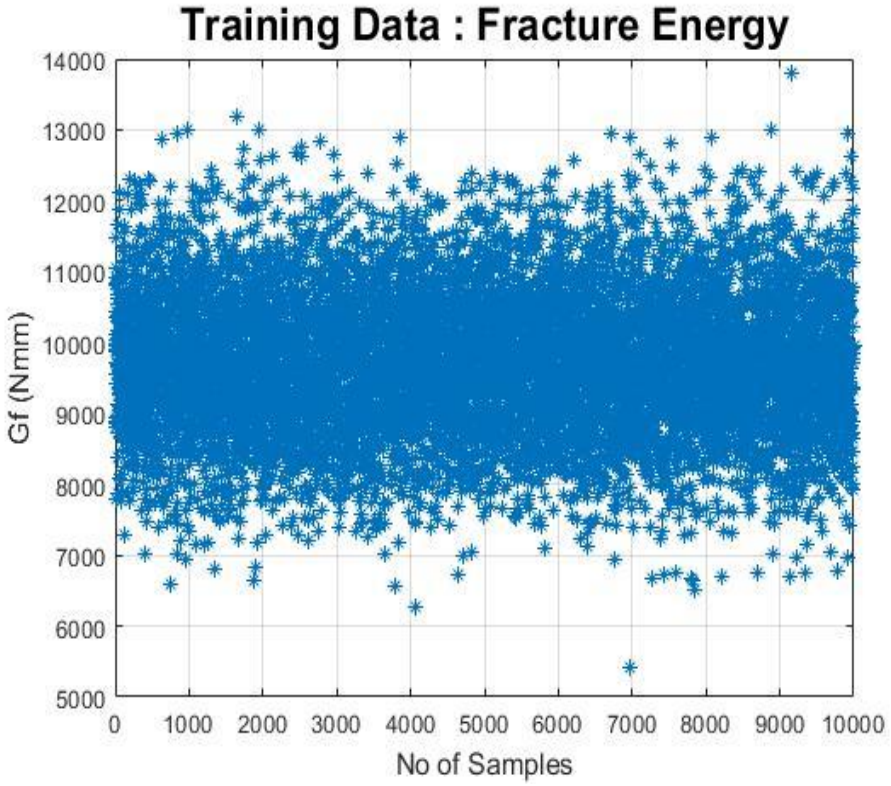

Figure 1.9 : Model Response : Fracture Energy(Gf) for N=10000 Training Samples

K_n (MPa/mm)	S_o (MPa)	δ_i (mm)	$\delta_f(mm)$	H $(MPa$ $/mm)$	v_o(mm/s)	Q(J)
162.3506	263.9073	10.5137	27.1465	10.1712	1.0123e-05	9.7923e-21

Table 1.2 : θ_{Gf}* : Predicted Input Parameters by KNN Regression based on Model Response : Facture Energy (Gf)

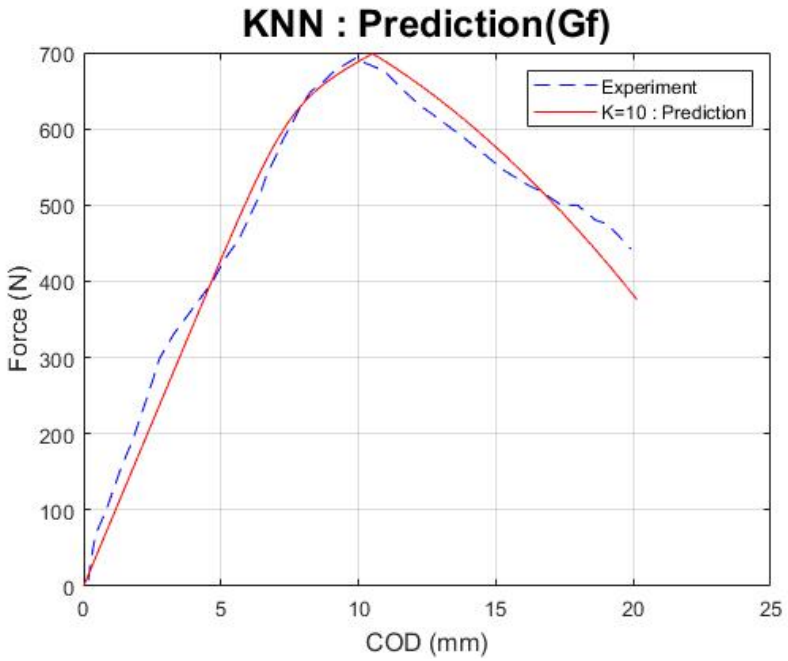

Figure 1.10 : Comparison of model prediction with the experiment for the F vs COD curve

Prediction Error: $(\frac{\mathrm{Ye}-Ym}{Ye})$ X $100 = 0.0627$

1.4.3.2 KNN Regression Results ,Model Output: Maximum Force (Fmax)

Figure 1.11 : Model Response : Fracture Energy(Fmax) for N=10000 Training Samples

K_n (MPa/mm)	S_o (MPa)	δ_i (mm)	$\delta_f(mm)$	H (MPa/mm)	v_o(mm/s)	Q(J)
176.2186	265.4165	10.3432	27.2683	10.5051	1.0018e-05	1.0279e-20

Table 1.3 : θ^*_{Fmax} : Predicted Input Parameters by KNN Regression based on Model Response : Maximum Force (Gf)

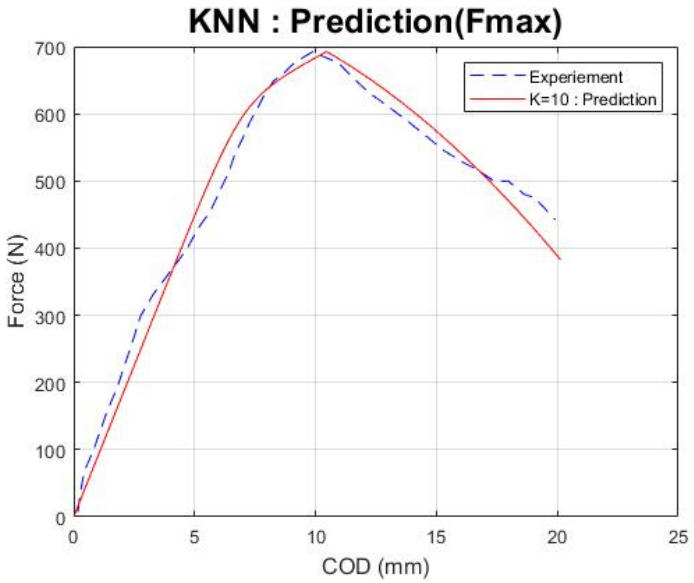

Figure 1.12 : Comparison of model prediction with the experiment for the F vs COD curve

Prediction Error: $(\frac{\text{Ye} - Ym}{Ye})$ X $100 = 0.0047$

1.4.3.3 KNN Regression Results, Model Output: Fracture Energy (Gf)

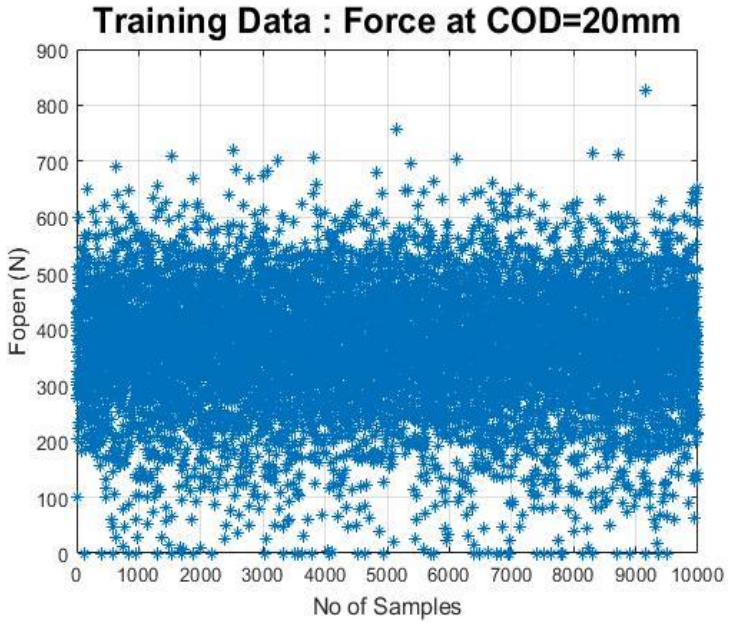

Figure 1.13 : Model Response : Force at COD =20 (Fopen) for N=10000 Training Samples

K_n (MPa/mm)	S_o (MPa)	δ_i (mm)	$\delta_f (mm)$	H $(MPa$ $/mm)$	v_o(mm/s)	Q(J)
172.2376	262.8948	10.3757	28.8303	9.9888	9.4330e-06	9.7067e-21

Table 1.4 : θ^*_{Fopen} : Predicted Input Parameters by KNN Regression based on Model Response : Force at COD=20 mm (Fopen)

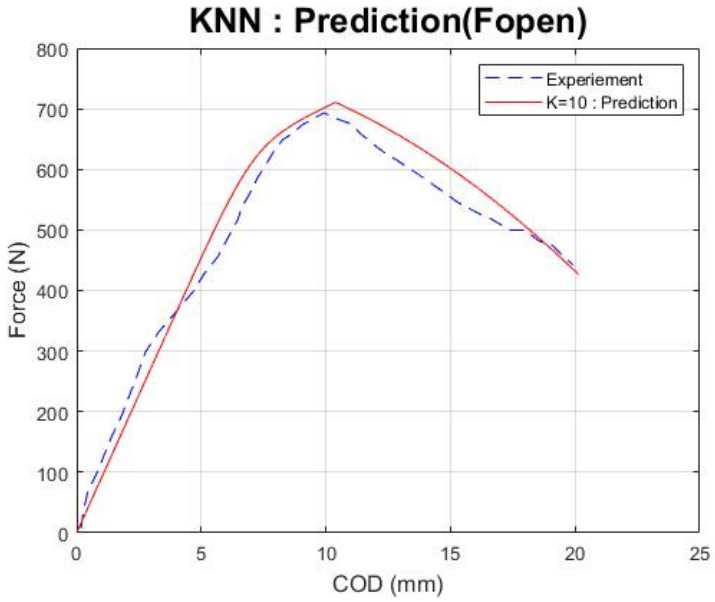

Figure 1.14 : Comparison of model prediction with the experiment for the F vs COD curve

Prediction Error: $(\frac{\text{Ye} - Ym}{Ye})$ X $100 = 1.9511$

1.4.3.4 KNN Regression Result

We take the mean of the prediction of input parameters for 3 model responses to compute the calibrated results.

K_n (MPa/mm)	S_o (MPa)	δ_i (mm)	$\delta_f(mm)$	H (MPa/mm)	v_o(mm/s)	Q(J)
170.2689	264.0728	10.41084	27.74839	10.22172	9.85825e-06	9.92619e-21

Table 1.5 : Predicted Input Values of Traction Separation Law for KNN Regression

1.5 Model Verification:

The predicted values of the traction separation law as mentioned in Table 1.5 were used to conduct the Numerical Simulation for RDCB specimen. The Force vs COD curve for based on the predicted values gave a good match with the experimental results. The KNN Regression Algorithm can train the model reasonably for the Quasi-Static Simulation with a Strain Rate: 5.08 mm/min. The Prediction Error based on the Fracture energy is calculated as :

$$\frac{\mathrm{G_{fe}} - G_{fm}}{G_{fe}}) \text{ X } 100 = 1.9511$$

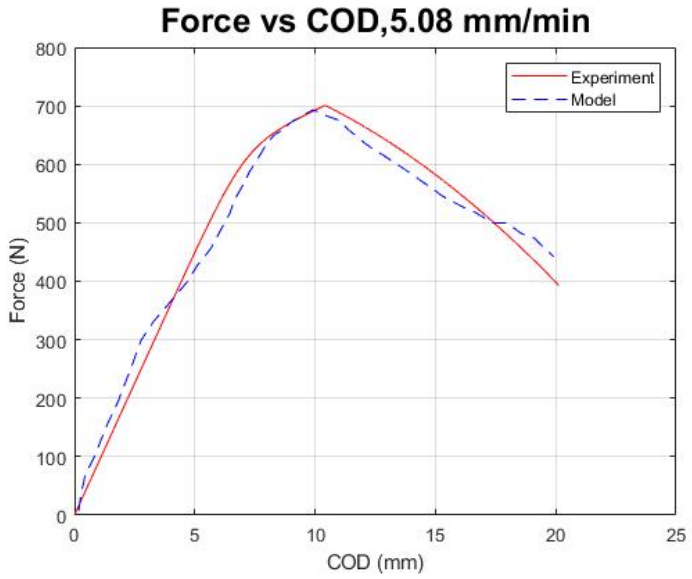

Figure 1.15 : Comparison of F vs COD curve between Predicted Model and Experiment

1.6 Model Validation:

The predicted model for $f(X, \theta^*)$ for a strain rate of 5.08 mm/min is Validated for High Strain Rates. The model must be updated for the strain rate and everything other input parameter employed for 5.08 mm/min is kept same. Strain Rate is deterministic input parameter since it can be measured while the experiment is being conducted.

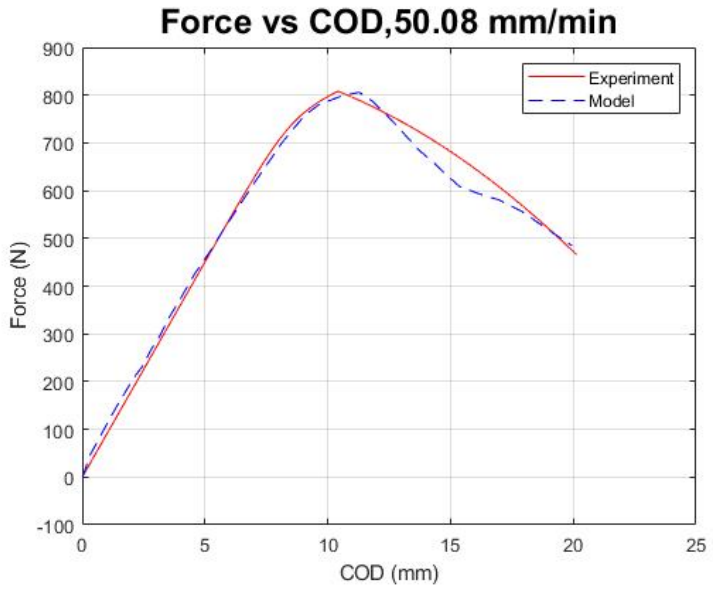

Figure 1.16 : Comparison of F vs COD curve between Predicted Model and Experiment for Strain Rate : 50.08 mm/min , Prediction Error % = 2.2924

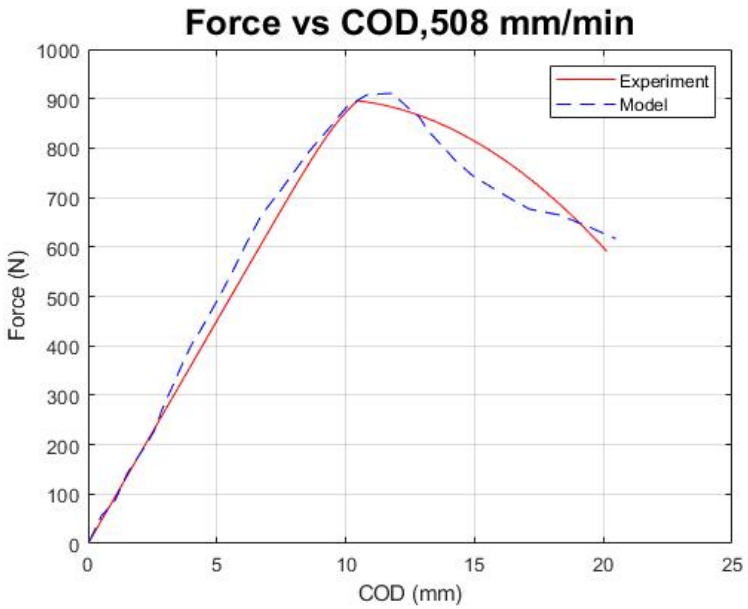

Figure 1.17 : Comparison of F vs COD curve between Predicted Model and Experiment for Strain Rate : 50.08 mm/min , Prediction Error % = 1.6439

2 Stochastic bond dissociation kinetics approach for a rate dependent Cohesive Zone Model

2.1 Abstract

The interface of a polymeric adhesive is composed of non-covalent bonds at molecular level which evolve during the fracture process. This evolution of bonds is assumed to be governed by the bonding probability (Stochastic) which varies based on the separation of the interface. Traction separation relationship have been developed [25] which are governed by the stochastic bond dissociation kinetics at the atomic and molecular level. The objective of this study is to develop stochastic bonding-based traction separation law which can characterize the failure of polymeric adhesives at both quasi-static and dynamic loading. The traction separation developed at the continuum level in previous study are taken as reference to calibrate the input parameters which govern the stochastic traction separation law. The model is verified and validated based on experiments conducted to quantify rate dependent mode-I fracture for high density polyethylene based thermoplastic adhesive. [19]

2.2 Background: Theory

The polymeric adhesives are composed of large number of bonding sites of non-covalent bond. A single bond complex is composed of a bond and a chain which are characterized by the bond potential energy U(r) and free energy E(x,t). The bond potential energy is a function of interatomic distance between two atoms and the free energy is function of separation distance between the interface caused by external loading. Bonding probability is defined as the fraction of closed bonds in a unit surface with a bonding site density $\rho(z)$ which is employed to get the traction separation relationship:

$$T(x,t;z) = \rho(z)b(x,t)\left(\frac{dE(x,t)}{dx}\right) \qquad 10$$

Where $T(x,t;z)$, $\rho(z), b(x,t), E(x,t)$ represent the Traction, Bond Density, Bonding Probability & Free Energy

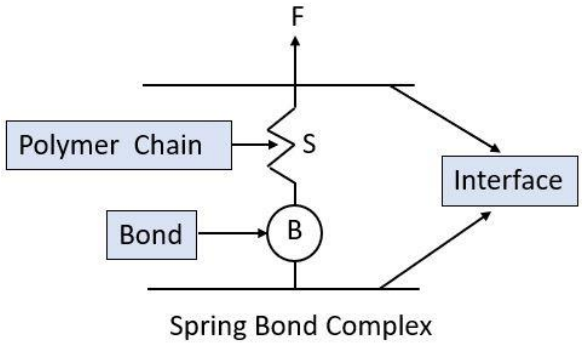

Figure 2.1 : Single Spring Bond Complex

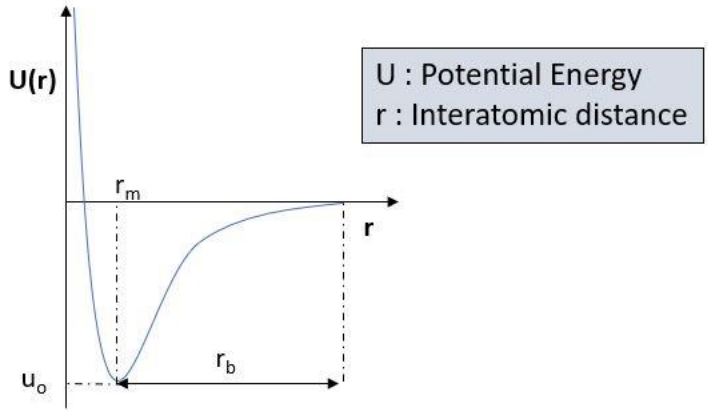

Figure 2.2 : Bond Potential Energy as function of interatomic distances

For a quasi-static loading, the bonding probability follows boltzmann distribution represented by the following equation:

$$b(x) = \frac{1}{1+exp\left(-\beta U(r(x))\right)}, \beta = \frac{1}{k_b T} \quad 11$$

where k_b is the boltzmann constant and T is the absolute temperature.

For dynamic loading, the bonding probability evolves based on the following equation:

$$b(x,t) = b_0 exp\left(-\frac{\beta k_{off} K_b x^3}{3V}\right) \quad 12$$

Where b_o, k_{off}, K_b, x, V represent the initial bonding probability when no traction is applied , off-rate which quantifies the transition of a closed bond to become ruptures in a unit time [26], bond Stiffness , interface separation and strain rate.

An expression for a strain rate dependent traction separation law for can be expressed based equations 10, 12:

$$T(x,t) = \rho b_0 K_b x exp\left(-\frac{\beta koff K b x^3}{3V}\right) \quad 13$$

where $\frac{dE(x,t)}{dx} = K_b x$

The following plots were generated based on Equations 12,13 and taking reference of stochastic traction separation parameters from [Ref]

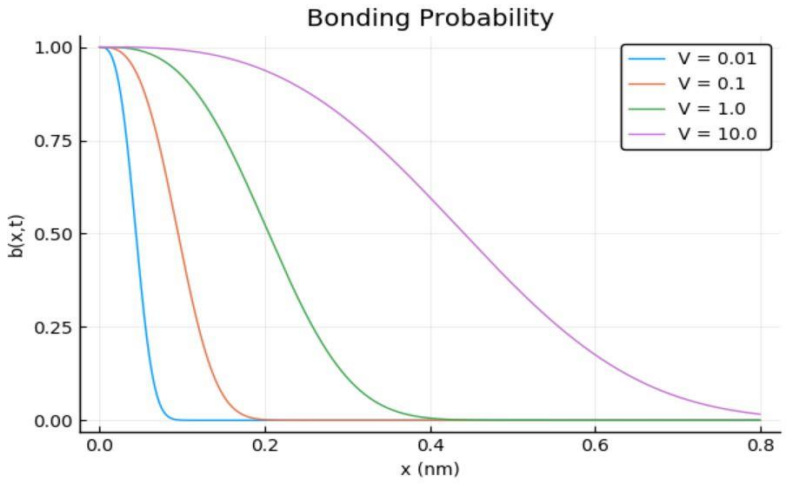

Figure 2.3 : Evolution of bonding probability at different Strain Rates (nm/sec)

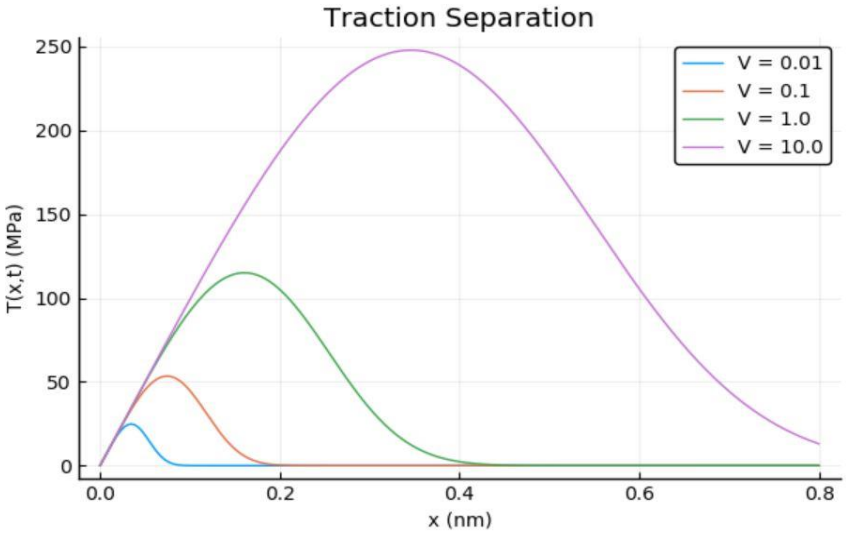

Figure 2.4 : Stochastic Traction Separation Law at different Strain Rates (nm/sec)

2.3 Stochastic Bonding Cohesive Law: Polymeric Adhesive

2.3.1 Calculation for Cohesive Law, Quasi-Static Strain Rate:5.08 mm/ min

The rate dependent traction separation law governed by stochastic bonding governed by Equation :13 is employed to estimate the Mode-I Fracture of HDP based thermoplastic adhesive . We employed a strategy to co-relate the calibrated traction separation curve for Quasi-Static Loading (5.08 mm/min) based on viscoplastic flow rule developed in Study 1 to calculate the parameters governing the stochastic bonding-based traction separation law. As mentioned in the previous section the expression rate dependent traction separation law is :

$$T(x,t) = \rho b_0 K_b x exp\left(-\frac{\beta k_{off} K_b x^3}{3V}\right) \quad 13$$

Parameter	Description
$\rho\ (bonds/m^2)$	Bond density
b_0	Initial bonding probability
$K_b\ (N/m)$	Single bond complex stiffness
$x\ (m)$	Interfacial separation
kb (J)	Boltzmann Constant
$t(K)$	Absolute temperature
$koff$	off rate
$V\ (m/s)$	Strain Rate

Table 2.1 : Parameters governing the stochastic bonding based rate dependent traction separation law

We took reference of all parameters mentioned in Table 2.1 for an adhesively joint interface [Ref] except the off rate : koff and Kb which we calculate by taking reference viscoplastic flow based traction separation law. An expression for maximum traction and separation at that value can be calculated by maximizing the function ($T(x,t)$) which is calculated as:

$$T_{max} = \rho b_0 K_b (3\alpha e)^{-\frac{1}{3}} \quad 14$$

$$x_{max} = (3\alpha)^{-\frac{1}{3}} \quad 15$$

where $\boldsymbol{\alpha} = \frac{\beta koff Kb}{3V}$ We extract the value of $Tmax$ and $xmax$ from the viscoplastic flow rule-based traction separation curve for strain rate 5.08 mm/min derived in Study 1 [Fig 1.5]. We can solve the two equations 14,15 to solve for $koff$ and Kb.

2.3.2 Results: Quasi-Static (Strain Rate: 5.08 mm/min)

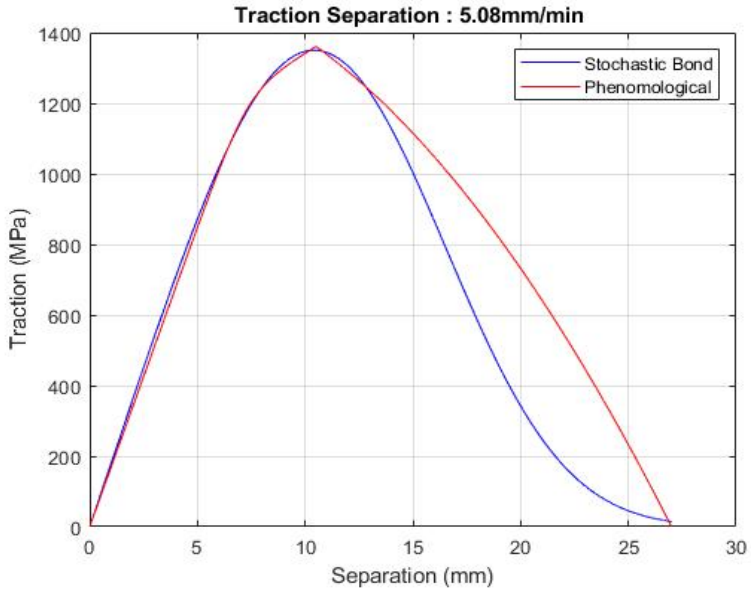

Figure 2.5 : Comparison of Stochastic-Bonding and Phenomenological (Viscoplastic Flow Rule) based Traction Separation Law for Strain Rate : 5.08mm/min

Parameter	Value
$\rho\ (bonds/m^2)$	10^{16}
b_0	1
$K_b\ (N/m)$	1.8085e-05
kb (J)	2.4720e+20
$t\ (K)$	300
$koff$	1.6482e-14
$V\ (m/s)$	8.3333e-05

Table 2.2 : Parameters stochastic bonding based rate dependent traction separation law for a strain rate : 5.08 mm/min

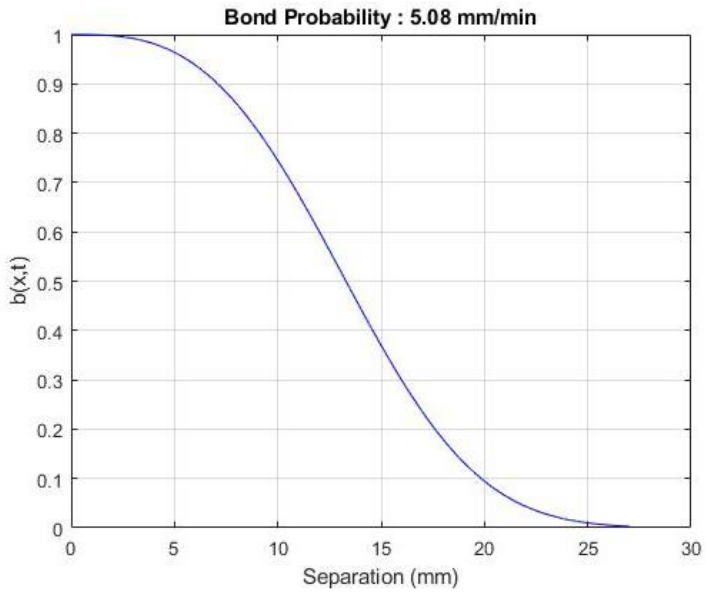

Figure 2.6 : Evolution of bonding probability as function of separation for a strain rate : 5.08 mm/min

The stochastic bonding-based traction separation curve is incorporated in the Numerical Simulation conducted for the RDCB specimen in reference to section 1.3.3 to plot force vs displacement curve and compared with mode-I fracture experiments for of HDP based thermoplastic adhesive

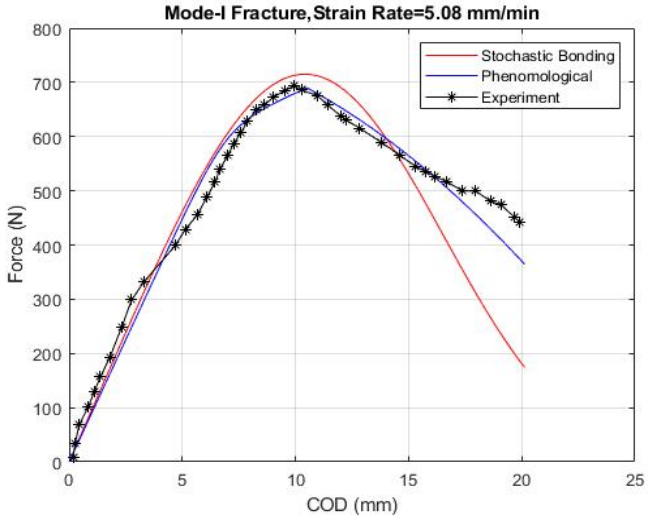

Figure 2.7 : Prediction of Stochastic-Bonding and Phenomenological (Viscoplastic Flow Rule) based Cohesive Laws for Mode-I Fracture , Strain Rate : 5.08 mm/min

2.3.3 Stochastic Bonding Cohesive Law Estimation for Higher Strain Rates

The traction separation law governed by stochastic bonding must be updated in response to higher strain rates. Based on Equation 13, we need to update the both Strain Rate (V) and off rate (koff) since both are a function of time. The off-rate is probability function which quantifies the transition chance of a closed bond to become ruptured in a unit time. The strain rate is an input parameter which is set by the user while conducting the double cantilever beam experiment and the off-rate needs to be updated based on the update in strain rate. For a strain rate of 50.08 mm/min ($V_{5.08}$) which is 10 times higher than the strain rate 5.08 mm/min ($V_{50.08}$), the traction ($T(x,t)$) gets scaled by a factor of ~ 2 assuming every other parameter except V in Table 2.1 remains unchanged. The prediction of stochastic bonding-based traction separation curve for was very poor when we compared with calibrated traction separation curve (viscoplastic flow rule) for higher strain rates. To account for the scaling factor for traction ($T(x,t)$) for higher strain we adjusted the off rate based on the following equation:

$$k_{off}^{V_2} = \left(\frac{V_2}{V_1}\right) * 0.75 * \ k_{off}^{V_1} \qquad 16$$

Where $V_2, V_1, k_{off}^{V2}, k_{off}^{V1}$ represent the high strain rate, quasi static strain rate , off-rate at V_2 , off-rate at V_1 respectively. Equation 16 is developed based on the calibrated traction separation curves (viscoplastic flow rule) for high strain rates (50.8 mm, 508 mm/min).

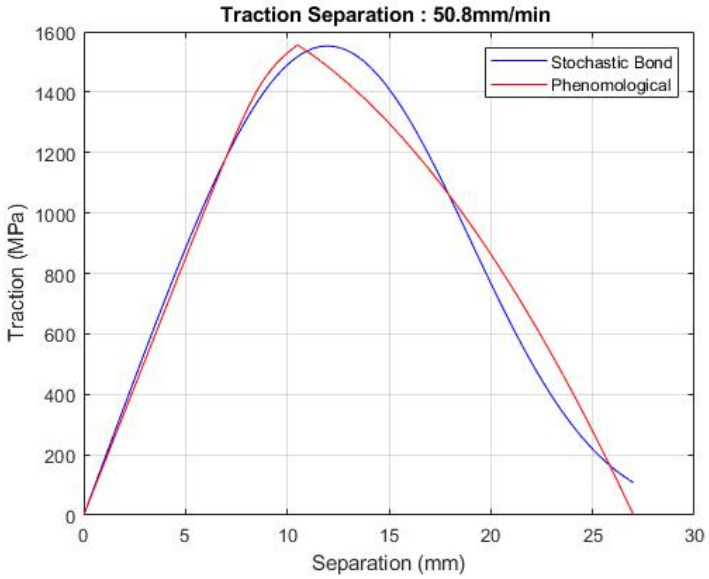

Figure 2.8 : Comparison of Stochastic-Bonding and Phenomenological (Viscoplastic Flow Rule) based Traction Separation Law for Strain Rate : 50.8mm/min

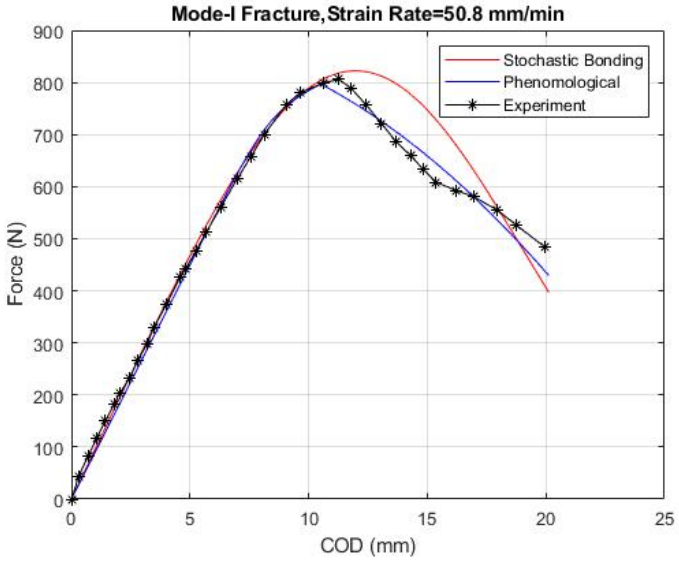

Figure 2.9 : Prediction of Stochastic-Bonding and Phenomenological (Viscoplastic Flow Rule) based Cohesive Laws for Mode-I Fracture , Strain Rate : 50.08 mm/min

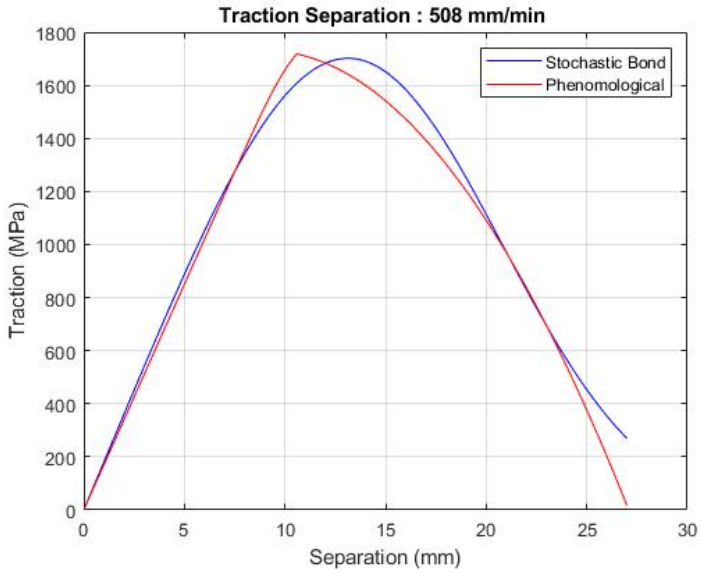

Figure 2.10 : Comparison of Stochastic-Bonding and Phenomenological (Viscoplastic Flow Rule) based Traction Separation Law for Strain Rate : 508mm/min

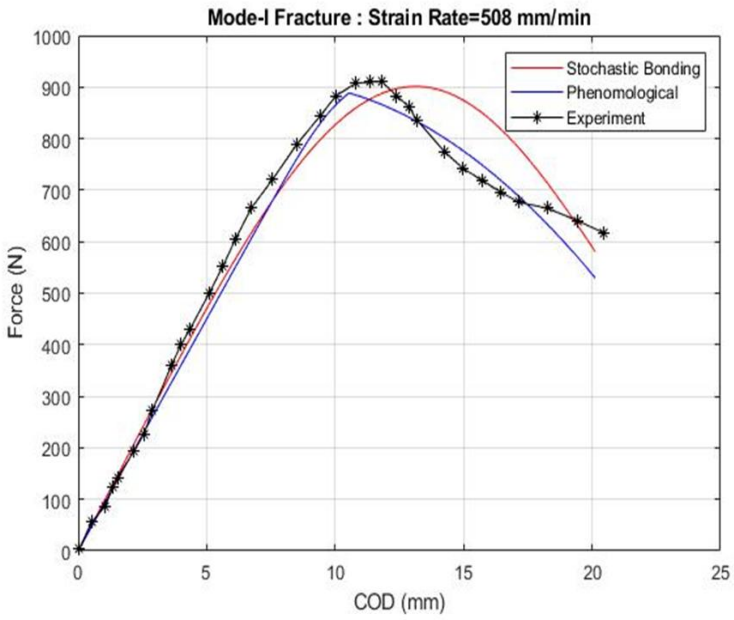

Figure 2.11 : Prediction of Stochastic-Bonding and Phenomenological (Viscoplastic Flow Rule) based Cohesive Laws for Mode-I Fracture , Strain Rate : 508 mm/min

2.4 Results

The rate traction separation law is estimated for 3 strain rates and validated for experimental results for Mode-I Fracture [Ref]. The error estimated employed to compare the Simulation and experimental results is Fracture Energy (Gf).

$$\%\ Error = \left(\frac{(|Gf_e - Gf_m|)}{Gf_e}\right) * 100$$

Where Gf_e, Gf_m represent Experimental Fracture Energy and Simulation Model Fracture Energy

Strain Rate (mm/min)	Error %
5.08	4.2644
50.8	5.0656
508	0.6036

Table 2.3 : Percentage Error for 3 strain rates

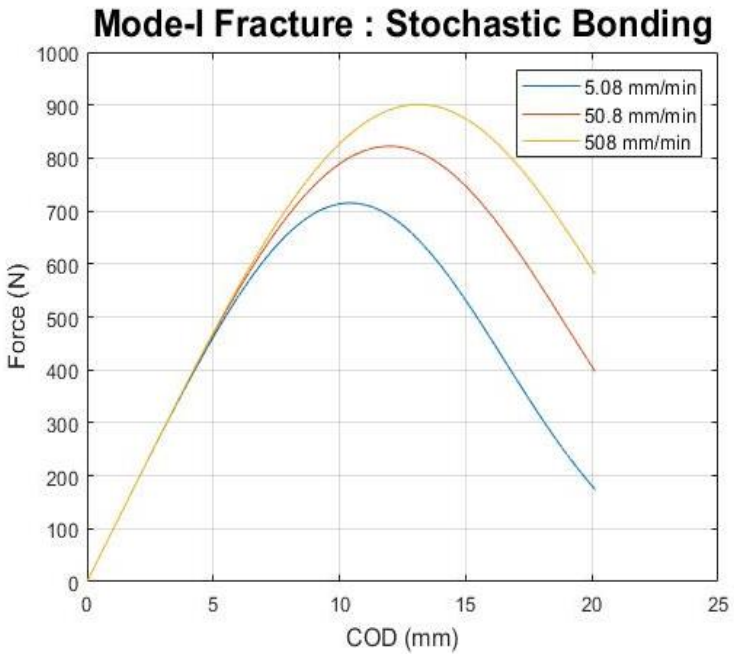

Figure 2.12 : Stochastic Bonding : Predicted Mode-I Fracture Response for 3 strain rates

3 Material calibration and Cohesive Zone Modelling approach to predict Interfacial Adhesion of Mussel Inspired Smart Adhesives

3.1 Abstract

Adhesives are polymer-based compounds with an ability to join dissimilar materials under specific conditions and have been extensively employed in numerous industrial applications such as manufacturing, medical etc. A smart adhesive inspired marine mussels has a characteristic property of reversible switching between adhesive and non-adhesive state by changing the pH level from acidic to basic respectively. This unique property was explored through a series of experiments to characterize the adhesive properties of different types of smart adhesives.[27]The experiments predict a force vs displacement plot based on a contact mechanics test for different pH levels. The aim of this study is to employ a numerical simulation for the contact mechanics test to predict the material response of smart adhesive by employing material calibration and cohesive zone modelling.

3.2 Introduction

Adhesives are polymeric compounds which forms adhesive bonds between two dissimilar materials based on numerous mechanisms such as adsorption, mechanical interlocking, interdiffusion and van der waal forces. Although they have numerous advantages such as uniform distribution of stress, reduction noise vibration and harshness levels, high strength to weight ratio, the application is limited due to difficulty in disassembly and weak bonding due to moist conditions. Adhesives with the ability to transition between strong and weak adhesion and maintain adhesion in marine environments will be extremely beneficial.

The observations for smart adhesives is in reference to research conducted by Dr Ameya Narkar [28]. Smart adhesives have been developed which demonstrate strong adhesion at acidic pH and weak adhesion at basic pH. Further, they demonstrate reversible action between their adhesive and non-adhesive state and strong adhesion at mildly basic pH typically observed in marine environments. Hybrid structures developed from polydimethylsiloxane and adhesive hydrogel showcased rapid switching adhesive states.

The present study focuses on the contact mechanics experiment conducted on adhesive hydrogel to predict adhesive strength by plotting force vs displacement curve at different pH level. The force vs displacement plot demonstrated a non-linear viscoelastic response and adhesive behavior during application of tensile load. Hyperelastic material models are employed to characterize non-linear stress strain response and a generalized Maxwell's model is employed to add strain rate dependent behavior into the material model. The adhesion is characterized by cohesive zone models by defining a traction

separation law which predicts Fracture in Mode -I, II. The primary objective is to develop a contact mechanics simulation which can characterize the material response of the adhesive by comparing the simulation result with the experimental results which is also termed as inverse calibration. The traction separation law is governed by a set of N input parameters which are non-deterministic in nature and require a probabilistic representation to perform uncertainty quantification. A sensitivity analysis conducted identifies the most critical parameters for this simulation which can be used for further calibration study for future simulations.

3.3 Experimental Results:

3.3.1 Contact Mechanics Test:

The experiment was conducted to characterize the adhesive strength of hydrogel at pH = 3 (acidic) and pH = 9 (basic) towards substrate: Borosilicate Glass. The adhesive hydrogel was a polymer consisting of dopamine meth acrylamide (DMA) and 3-acrlyoamido phenylboronic acid(AAPBA).The experimental setup included an indentation device powered by a stepper with the hollow hemispherical sample of adhesive hydrogel fixed to a steel indenter. The indenter was compressed against the substrate at a strain rate 1µm/sec till a compressive load of 20 mN was reached. At this point the indenter is retracted back at the same strain rate till the adhesive strength is completely diminishes. This experiment was conducted for both pH = 3 (acidic) and pH = 9 (basic) by changing the pH buffer solution at contact surface between the adhesive and substrate. [27]

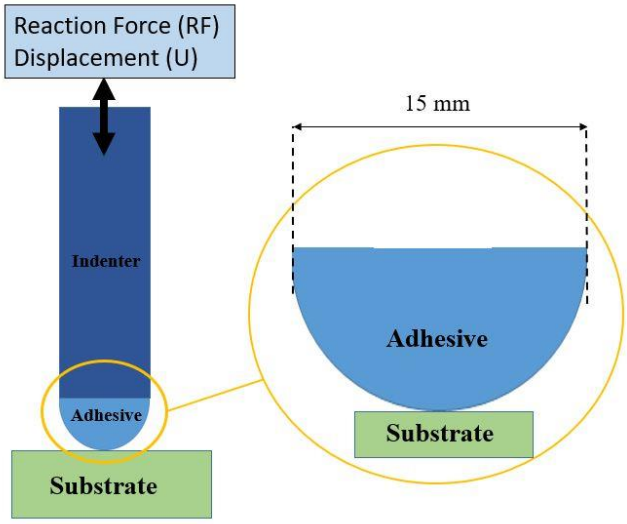

Figure 3.1 : Schematic of Contact Mechanics Experiment Conducted to characterize interfacial binding property of adhesive hydrogel

3.3.2 Experimental Results: Force vs Displacement Plot

A force vs displacement graph was plotted based on the contact mechanics test to calculate the work done by the adhesive and maximum adhesive force. The plots demonstrated ~8-10 times higher adhesion at acidic pH as compared to basic pH. Also, the loading/ unloading cycle observed Force-Displacement curve showcased a non-linear viscoelastic response of the adhesive hydrogel. The adhesion was observed after the indenter retracted back to its base state when the compressive force is zero. After the indenter reaches this state, tensile force had to be applied to break the bonds formed between the hydrogel and the substrate. The experimental results shown below is for Adhesive prepared with 10 mol % each of DMA and AAPBA.

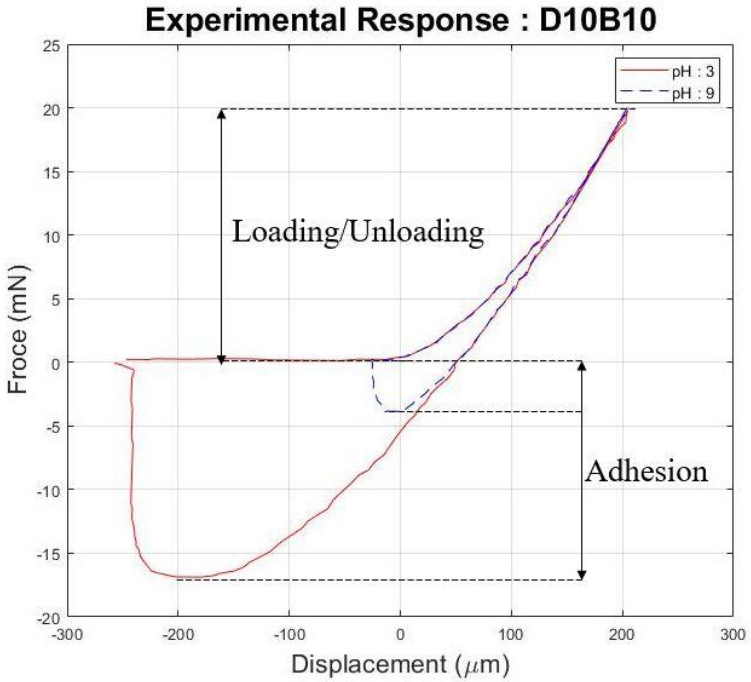

Figure 3.2 : Force vs Displacement Plot : Adhesive (D10B10)

3.4 Numerical Simulation: Contact Mechanics Test

A numerical simulation has been setup for the experimental contact mechanics test in Abaqus Implicit to predict material response of the adhesive hydrogel. The material parameters for the adhesive are inversely calibrated based on the experimental force vs displacement in reference in to Figure 3.2. Based on the observation of the experimental response, we decided to divide the simulation into two procedure. The first procedure will characterize the non-linear viscoelastic material behavior based on the hyperelastic

material model and generalized maxwell model respectively. The second procedure will focus on employing the surface based cohesive zone model to prediction of adhesive behavior of the hydrogel with the substrate.

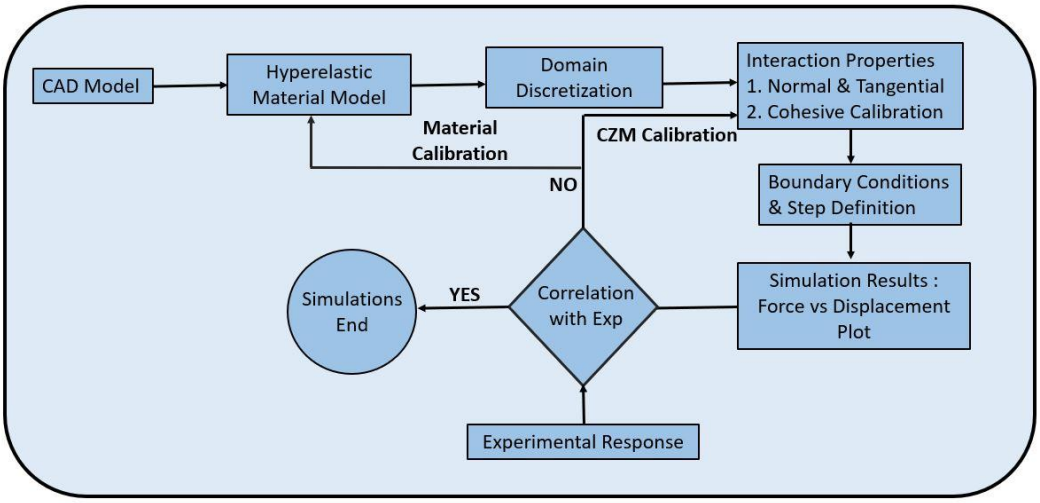

Figure 3.3 : Schematic Diagram for Inverse Calibration of Material Response of Adhesive Hydrogel conducted in Abaqus Implicit

Figure 3.3 represents the inverse calibration approach followed to conduct the numerical simulation for the contact mechanics test. The first step is to create a part representing the indenter, adhesive, substrate and assign material to each part respectively. The parts are assembled which defines a computational domain represented by finite elements. A 2d mesh is generated and a surface to surface contact is defined between the adhesive and substrate. Since we are employing a surface based cohesive zone model, the damage initiation and evolution conditions are defined as a contact interaction property. The contact mechanics simulation is a boundary value problem which requires defined dirichlet boundary conditions to be solved. The dirichlet boundary conditions for this non linear problem are the displacement boundary conditions in the simulation. Also we defined a multistep simulation to represents simulation scenarios: loading, unloading and adhesion. The output of the simulation is the force vs displacement curve which is compared to the experimental results. The model response is driven by material parameters (hyperelastic and viscoelastic) and cohesive zone parameters (traction separation law) which can be calculated by inverse calibration by predicted an accurate model response. The simulation is executed for different iterations of input parameters till the model response is in coherence with the experimental force vs displacement curve

3.4.1 Simulation Setup Abaqus

The objective of the contact mechanics simulation is to apply the concepts of computational mechanics to predict material response of smart adhesives through correlation with the experimental results. This simulation will solve a set of non-linear equations in Abaqus implicit which arise due large deformation in elastomers and surface based cohesive zone models. The part assembly consists of an indenter with a hemispherical shaped adhesive affixed at the bottom which is in contact with the substrate. The material properties of steel and borosilicate glass are assigned to indenter and substrate respectively. Hyper elastic material model is assigned to the adhesive and the input parameters are inversely calibrated. The simulation possess asymmetry about the y-axis so linear axisymmetric elements are used with hybrid formulation. A hybrid formulation is employed nearly incompressible materials such as elastomers which includes an additional degree of freedom to compute stress since a pure displacement-based formulation causes volumetric locking. A surface to surface contact with small sliding formulation is defined between the adhesive and the substrate. The contact property includes definition of normal, tangential, cohesive behavior and damage model. The cohesive behavior requires the interfacial stiffness in normal and tangential direction as input and damage model requires the interface separation/stress at damage initiation and the fracture energy/final displacement at complete failure as inputs which basically the traction separation law. A node set must be defined to represent the surface area of adhesive bonded to the substrate in which the cohesive zone model is deployed to depict failure due application of external force. A solver based on solving implicit dynamic problems is invoked to solve the given non-linear problem.

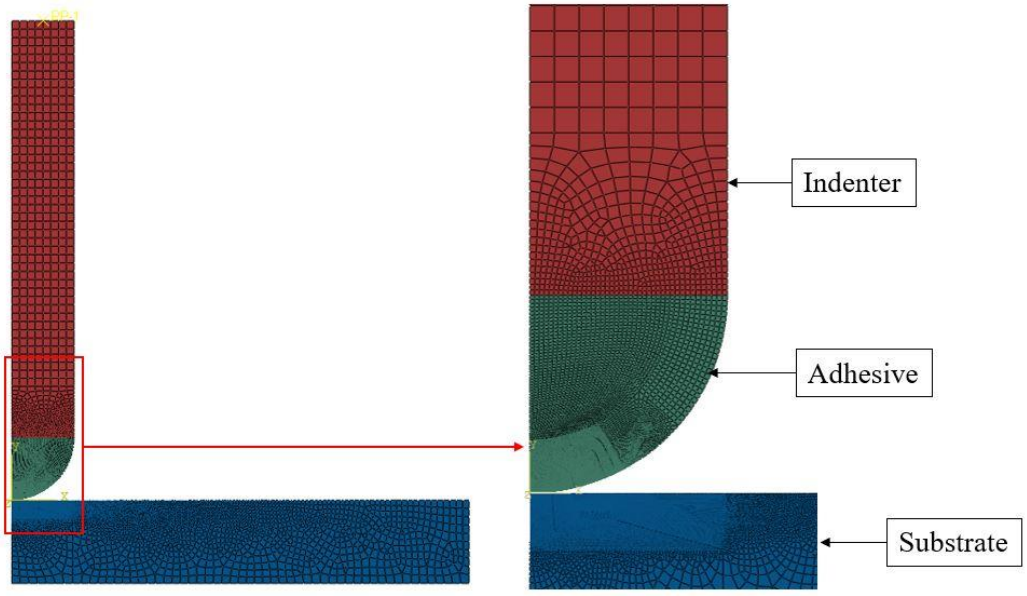

Figure 3.4 : Mesh Generated with linear axisymmetric elements: CAX3H , CAX4RH

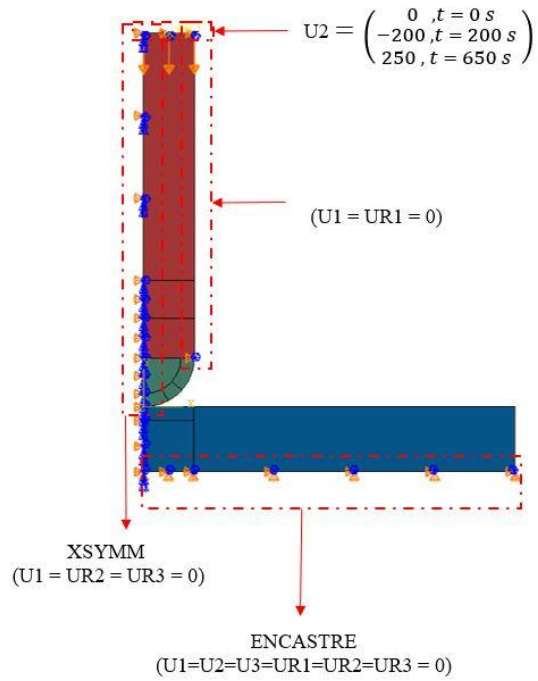

Figure 3.5 : Part Assembly with Boundary Conditions

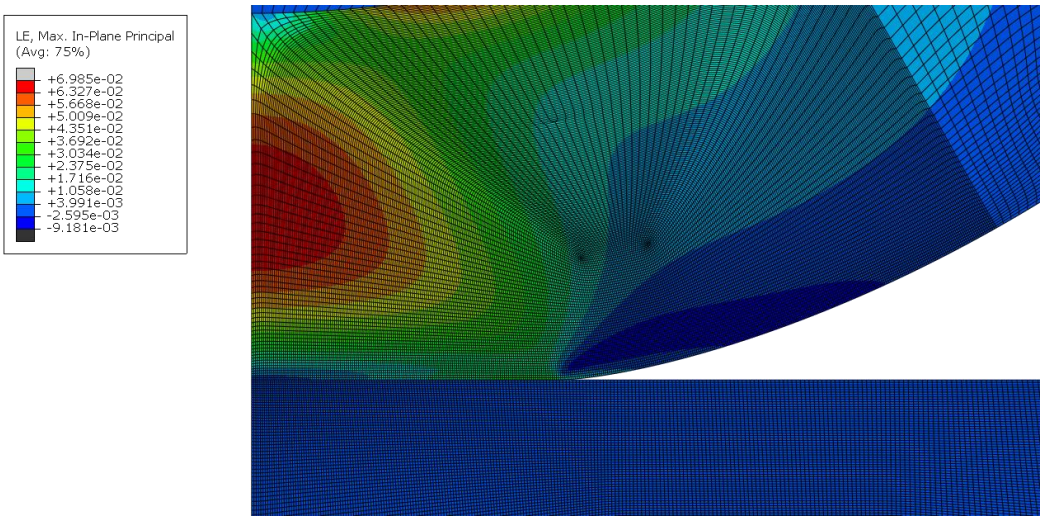

Figure 3.6 : Contour : Max in-plane principal logarithmic strain

3.5 Material Calibration

3.5.1 Hyperelastic Material Model

Elastomers typically undergo large deformation and a simple modulus of elasticity is not sufficient to define their stress-strain response. The constitutive material law governing hyperelastic material models can predict highly non-linear stress – strain behavior observed in elastomers. [29] A strain energy potential which is defined as the strain energy stored per unit reference volume as a function of strain at that point in the material is employed to characterize stress-strain response for finite deformations[30]. The general form of strain energy potential is given by the following equation:

$$U = \sum_{i,j=0}^{N} C_{ij}\,(I_1 - 3)^i (I_2 - 3)^j + \sum_{i=0}^{N} \frac{1}{D_i} (Jel - 1)^{2i} \qquad 1$$

where $U, C_{ij}, I_1, I_2, D_i, J_{el}$ represent strain energy potential, material parameters for deviatoric stress , first deviatoric strain invariant , second deviatoric strain invariant, material parameters for volumetric stress, elastic volume ratio. Different forms of the strain energy potential yields different material models such as Neo-Hookean, Mooney Rivlin, Ogden, Arruda Boyce. To characterize the material response of elastomers the hyperelastic material relies on curve fitting based on material data by conducting Uniaxial, Biaxial, Planar, Compression. An alternative technique is to assume a strain energy potential and inversely calibrate to predict material parameters that give a reasonable to fit to the experimental results. We will follow the second approach since we do not have material test for the adhesive hydrogel and predict material parameters based on inverse calibration employing experimental force vs displacement curve.

An Arruda-boyce hyperelastic material model is denoted as an eight chain-model as it originated from a representative volume element where eight springs emanate from the center of a cube to its corners. [31]This material model can accurately predict material response of most elastomers with limited test data. The deviatoric part of the equation is only dependent on the first invariant. The equation governing the Arruda Boyce model is

$$U = \mu \sum_{i=1}^{5} \frac{C_i}{\lambda_m^{2i-2}} \left(I_1 - 3^i\right) + \frac{1}{D}\left(\frac{(J_{el}^2 - 1)}{2} - lnJ_{el}\right) \qquad 2$$

where μ, λ_m *represent shear modulus and locking stretch*

We chose arruda boyce model to characterize the non-linear response of the adhesive hydrogel. This material model requires 3 parameters as input from the user λ, K, μ_0 which are locking stretch (Stretch value at which the slope of stress-strain curve rises significantly) , Bulk modulus ($K = \frac{2\mu(1+\nu)}{3(1-2\nu)}$, $\nu = 0.49$) and initial shear modulus. We

took some reference from [32] to start with an initial guess for the material parameters mentioned above and compared the simulation result: force vs displacement plot with the experiments. We updated the material parameters based on inaccurate the fit till the iteration when the material response was reasonably accurate with experiments.

Case	μ (MPa)	λm	K (MPa)
1	0.0017	30	0.0844
2	0.0087	30	0.4321
3	0.0050	30	0.2483
4	0.0075	30	0.3725
5	0.0100	30	0.0497

Table 3.1 : Arruda Boyce material parameters to perform inverse calibration.

The material parameters for case 4 gave best match to the experimental results

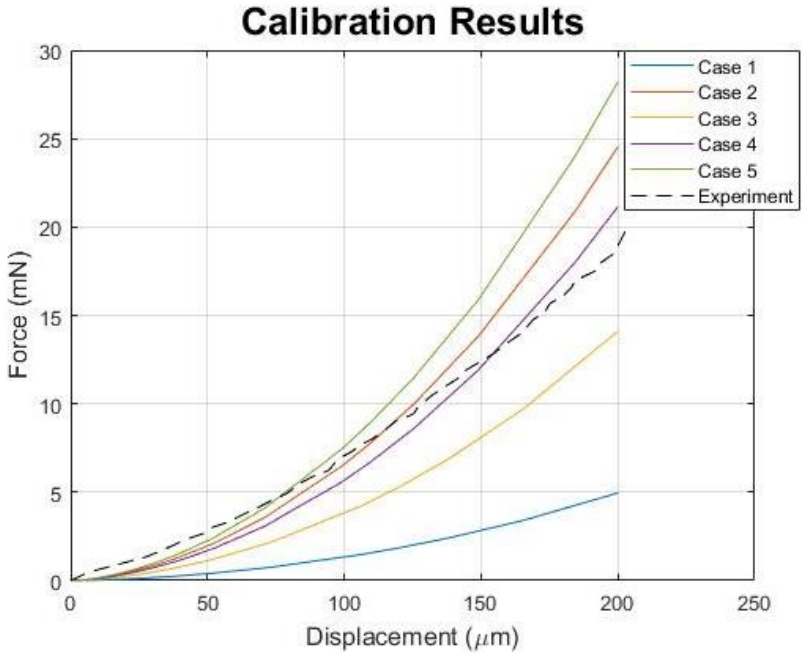

Figure 3.7 : Arruda Boyce material model calibration results for different iterations

3.5.2 Viscoelasticity

Polymers demonstrate viscoelastic material response owing to frictional sliding between heavily cross-linked molecular chains which causing viscous dissipation of heat. [Ref] Experiments such as Creep, Stress Relaxation and Dynamic Mechanical Analysis are conducted to characterize the viscoelasticity. The experiment applies a time varying load to a given material and stress , strain is measured. For a viscoelastic material, strain lags stress. The stress component in phase with strain represents elastic strain energy while the stress component out of phase with strain represents strain energy lost in viscous dissipation. The in-phase modulus is known as storage modulus (G') and out of phase modulus(G'') is known as loss modulus. [33]

Oscillatory rheometry conducted on adhesive hydrogel for both acidic and basic pH reported storage modulus (G') 1-2 orders magnitude higher that the loss modulus (G'') indicating viscoelastic behavior due to chemical crosslinking [27]. To predict the viscoelastic response in a numerical simulation a generalized maxwell model which is also termed as maxwell-wiechert model is employed [34]. This model is composed of a non-linear spring and a number of maxwell elements composed of a spring and dashpot arranged in a parallel. This model accounts for molecular segments with different lengths having different stress relaxation times which helps in accurate representation of the viscoelastic behavior of polymers.

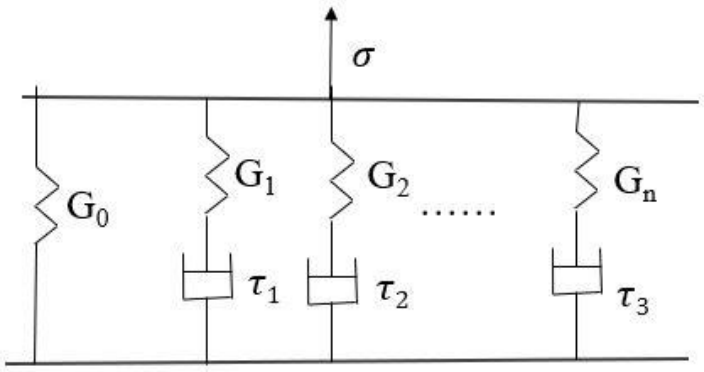

Figure 3.8 : Maxwell and Weichert Model

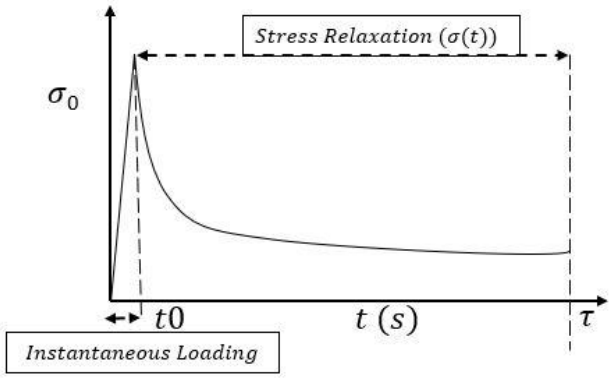

Figure 3.9 : Stress Relaxation Experiment

A Prony series is defined to represent the maxwell-weichert model which is represented by the following equation:

$$G(t) = Go\left(1 - \sum_{i=1}^{N} g_i\left(1 - e^{-\left(\frac{t}{\tau_i}\right)}\right)\right), g_i = G_i(t)/\ Go \qquad 3$$

where $Go, G_i(t), g_i, \tau,$ represent initial modulus (μ or K) , relaxation modulus as function of time, ratio between relaxation modulus & initial modulus and relaxation time. The parameters for prony series can be calculated based on experiments: creep, stress relaxation and DMA or by performing inverse calibration. We performed inverse calibration to calculate the prony series parameters that gave a good fit with the experimental results. We observed that 3 maxwell elements were able to give a good prediction

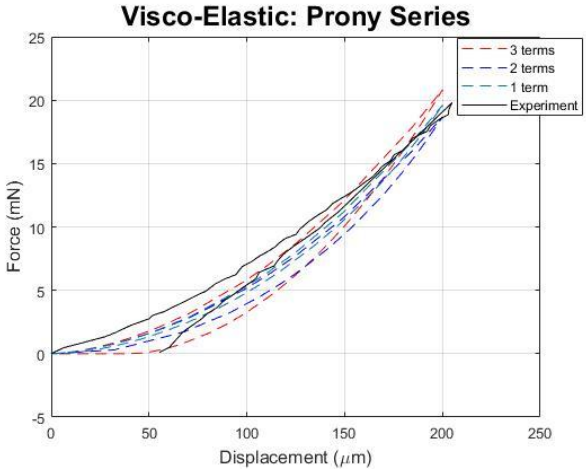

Figure 3.10 : Comparison of viscoelastic response with experiments considering the number of maxwell elements (no. of terms in prony series)

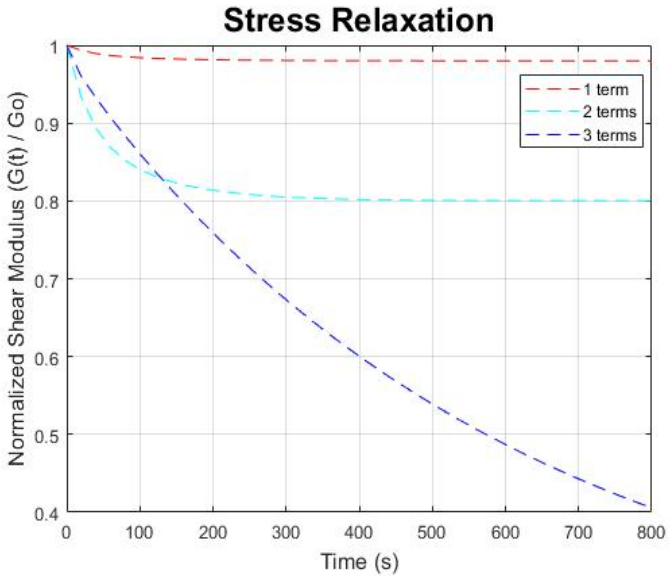

Figure 3.11 : Stress Relaxation comparison between number of maxwell elements

3.5.3 Material Calibration Results:

Arruda Boyce hyperelastic material model along with Maxwell & Weichert Model for viscoelasticity gave a reasonably good fit with the experimental results. The calibrated material parameters are as mentioned below.

μ (MPa)	λ_m	K (MPa)
0.0082	30	0.4703

Table 3.2 : Hyperelastic material parameters

Maxwell Unit	gi	ki	τ (s)
1	0.01	0.01	1
2	0.01	0.01	30
3	0.78	0.78	600

Table 3.3 : Viscoelastic material parameters

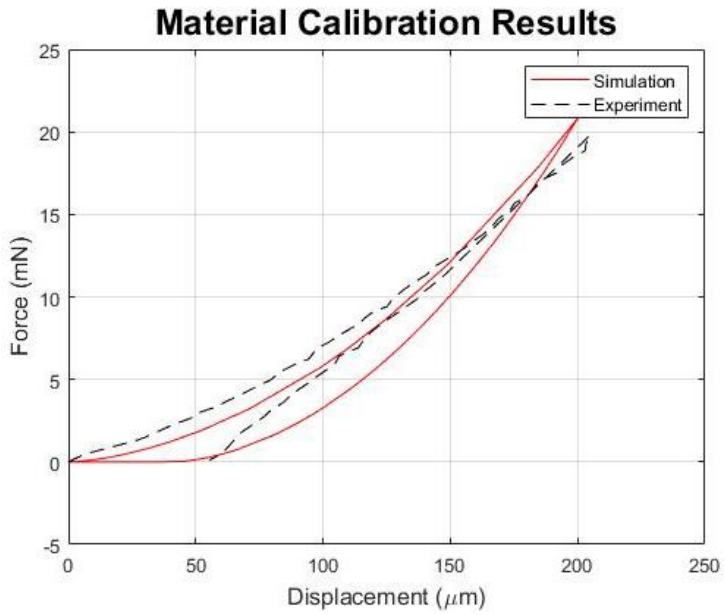

Figure 3.12 : Simulation prediction based on material parameters in Table 3.2,3.3

3.6 CZM parameters Calibration

3.6.1 Cohesive zone modelling

The interfacial failure is caused by relative sliding and opening of the interfaces which are bonded by polymeric adhesive. Fracture can be defines in Mode-I,II& III which represent crack initiation & propagation occurring due load applied in normal, shear directions respectively.

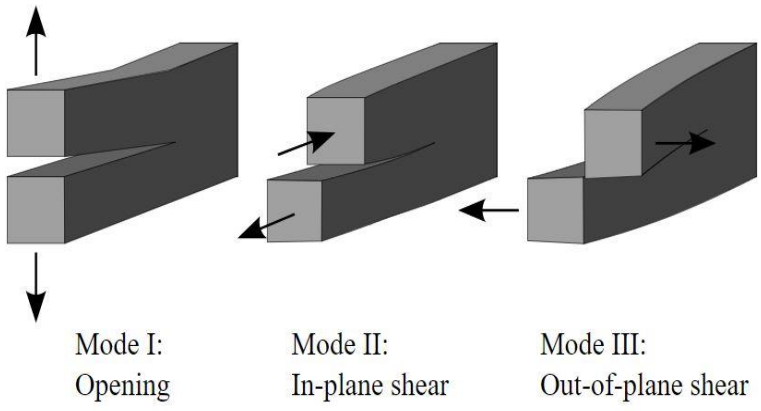

Figure 3.13 : Diagrams to depict failure modes [37]

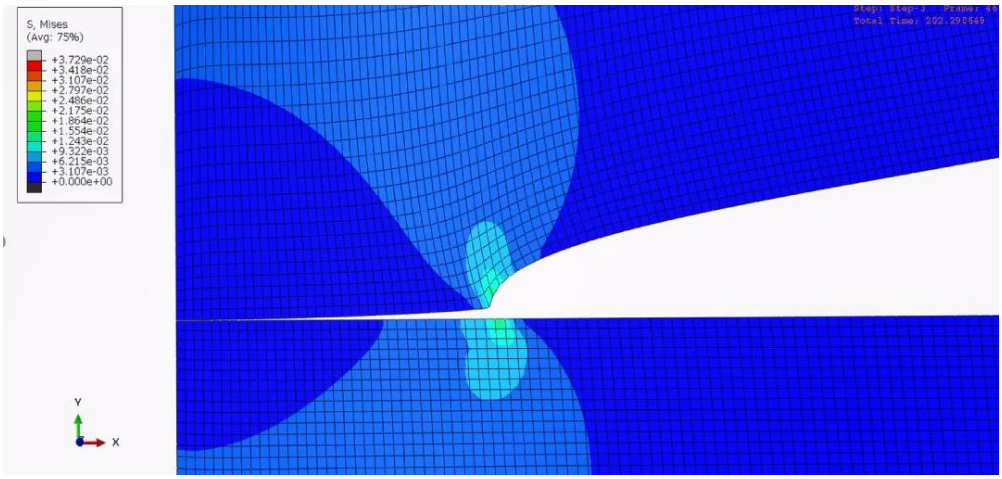

Figure 3.14 : Interfacial failure of polymeric adhesive

Cohesive zone models define a "process zone" in which fracture occurs due to relative opening sliding and opening of interface bonded by the adhesive [35]. It is an effective method to characterize nonlinear fracture occurring due to high plastic deformation. The constitutive cohesive law to predict failure is the traction separation relationship which defines the surface traction at the interface as a function of separation between them. The traction separation law is composed of two stages of failure: crack initiation and crack propagation which are defined by the following equation:

$$T(\delta) = \begin{pmatrix} K\delta \ , \ 0 < \delta < \delta i \ , \ Crack\ Initiation \\ (1-D)K\delta \ , \delta_i < \delta < \delta_f \ , \ Crack\ Propagation \end{pmatrix} \quad 4$$

$$D = \frac{\delta(\delta_f - \delta_i)}{\delta_f(\delta - \delta i)}, \delta_i < \delta < \delta_f \ , Damage\ Variable \quad 5$$

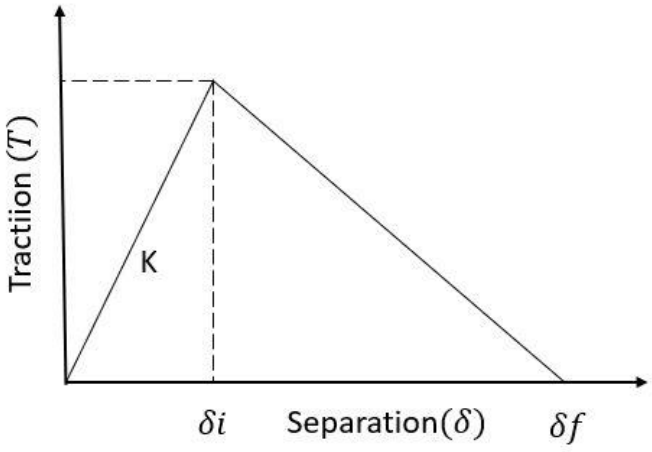

Figure 3.15 : Pure Mode I,II,III Bilinear Traction Separation Law

Equation 4 is a general expression for the traction separation which can be defined separately for failure modes in normal and shear direction. It is assumed that the material response till damage initiation is linear elastic followed by cohesive stiffness degradation based on a linear or exponential variation of damage variable which can be defined by final displacement at complete separation or the fracture energy which is defined by the area under the traction separation curve. A mixed mode fracture can be defined by defining fracture energy proportions in normal and shear directions. The above formulation is defined for surface based cohesive behavior which assumes negligible thickness of the adhesive. It can be defined as a contact surface interaction property during contact simulation setup in Abaqus. This assumption eliminates the procedure to generate the stiffness matrix for the adhesive layer. To account for thickness of the adhesive, a cohesive element-based formulation can be employed.

3.6.2 CZM parameter calibration

We chose a surface based cohesive law to characterize the adhesive strength of the hydrogel with an assumption that thickness of the adhesive is no influencing the fracture response. The simulation is being conducted in 2d, so we define a mixed mode fracture based on traction separation laws for Mode-I, II. The traction separation law is defined as surface interaction property for surface to surface contact formulation in Abaqus. A bonding node set must be defined which represents surface contact area of the adhesive hydrogel bonded with the substrate. We had assumed different sets of input parameters to calculate the traction separation law which gave a reasonable fit to the experimental results.

Sno	CZM Parameter	Description	Case 1	Case 2	Case 3
1	K_n (MPa/mm)	Normal Stiffness	5.0	5.0	5.0
2	δ_{ni} (mm)	Normal Opening at Damage Initiation	0.005	0.010	0.001
3	δ_{nf} (mm)	Normal Opening at Failure	0.010	0.020	0.002
4	K_t (MPa/mm)	Tangential Stiffness	5.0	5.0	5.0
6	δ_{ti} (mm)	Tangential Opening at Damage Initiation	0.005	0.005	0.005
7	δ_{tf} (mm)	Tangential Opening at Failure	0.010	0.010	0.010

Table 3.4 : Input Parameters governing the surface based traction separation law

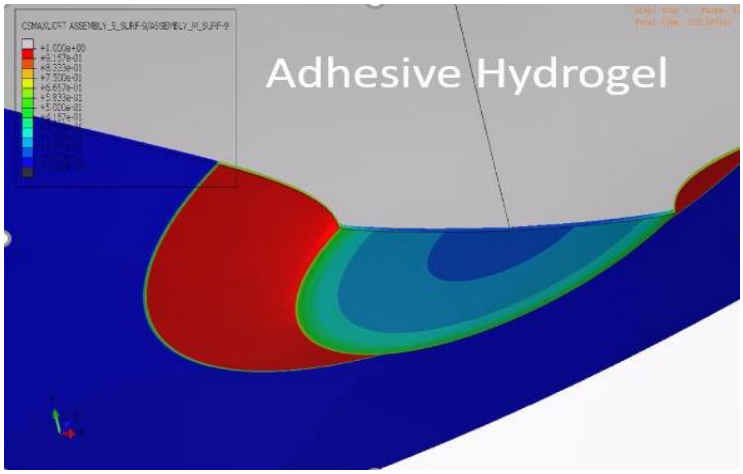

Figure 3.16 : Damage Progression of Adhesive, Red contour indicates complete debonding of adhesive from substrate

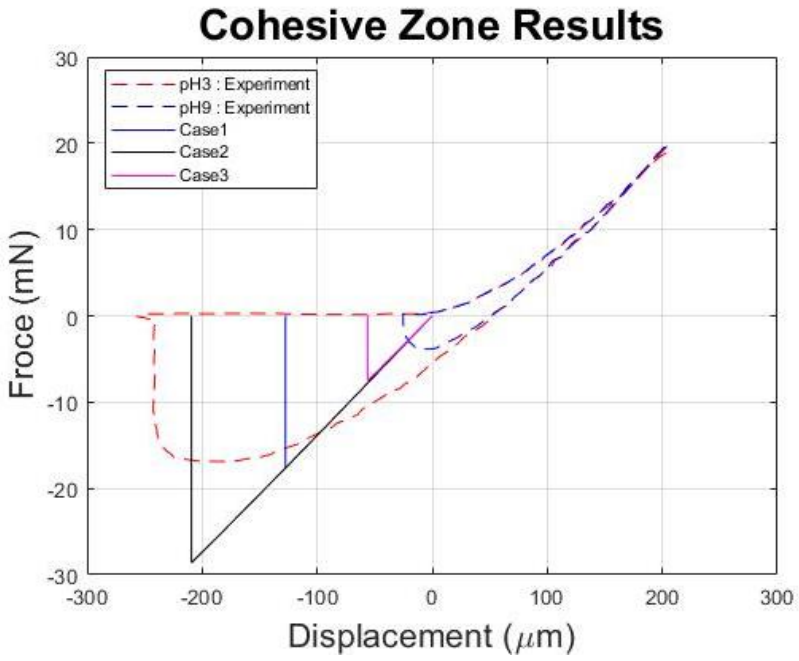

Figure 3.17 : Comparison of adhesive strength predicted by cohesive law with the experiments

Sensitivity Analysis

The traction separation to predict the adhesive strength is dependent upon six independent input parameters which are non-deterministic in nature since these parameters can't be measured experimentally. As demonstrated in the section 3.6 these CZM input parameters must be inversely calibrated based on the experimental results. A unique value for CZM parameters does not exist since any permutation of the input parameter set can give a reasonable match to the experimental response. Therefore, the estimation of non-deterministic CZM parameter requires a probabilistic interpretation in which we define a probability distribution function to quantify the uncertainty inherently present in the input parameters. The computational model employed for the contact mechanics simulation is given as

$$Y^m = f(\theta) \text{ where } \theta = \left[K_n\,, \delta_n\,, \delta_{nf}, K_t\,, \delta_t, \delta_{tf}\right] \quad 6$$

where Y^m is the model response which is fracture energy (G_f) in our numerical simulation. Sensitivity Analysis is the first step for uncertainty quantification which is conducted to determine the impact of variation of input parameter to the output results. Mathematically, it can also be defined as the partial derivative of the output function with respect to the input parameter at a specific value. [36]

Steps to conduct the sensitivity analysis:

1. Computational Model $Y^m = f(\theta)$.
   - Y^m: Model Response is Fracture Energy ($\int \mathbf{Fd\delta}$)
   - θ : Non Deterministic Input Parameters
2. Sensitivity Analysis:
   a. Impact of Variation of CZM parameters based on Fracture Energy
   b. Assume Normal Probability Distribution: $\theta \sim (\mu, \sigma^2)$
3. Calculate Reference Response: $Y^m_{ref} = f(\theta_{mean})$
4. Minimum Response : $Y^m_{min} = f(\theta i_{min},\ \theta j_{mean})\,,\ j \neq i$
5. Maximum Response : $Y^m_{min} = f(\theta i_{min},\ \theta j_{mean})\,,\ j \neq i$
6. Swing: |Yi max –Yi min|, sorted in descending order

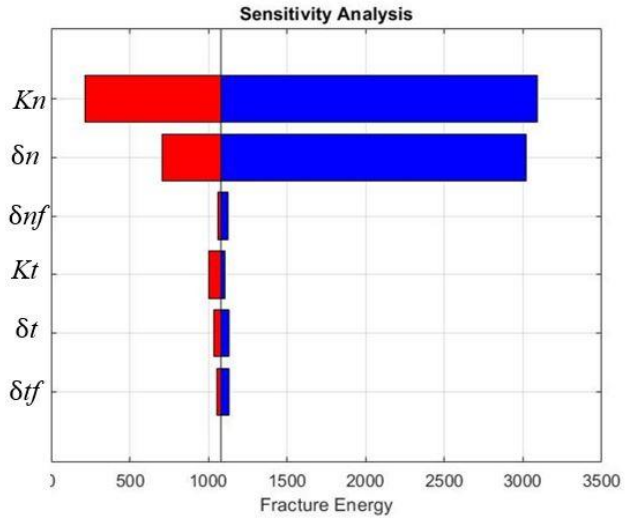

Figure 3.18 : Tornado diagram for sensitivity analysis

A deeper insight was gained into the effect of CZM parameters on fracture energy and concluded that failure of adhesive hydrogel is predominant in Mode – I which is a useful interpretation for future work for CZM parameter calibration

3.7 Results & Discussion

Based on the study conducted in section 3.5,3.6,3.7, an inversely calibration of the material parameters was performed for the adhesive hydrogel for both acidic and basic pH. The error estimation is computing the work done by the adhesive during the entire contact cycle. The work done is calculated as the area within the stress strain curve.

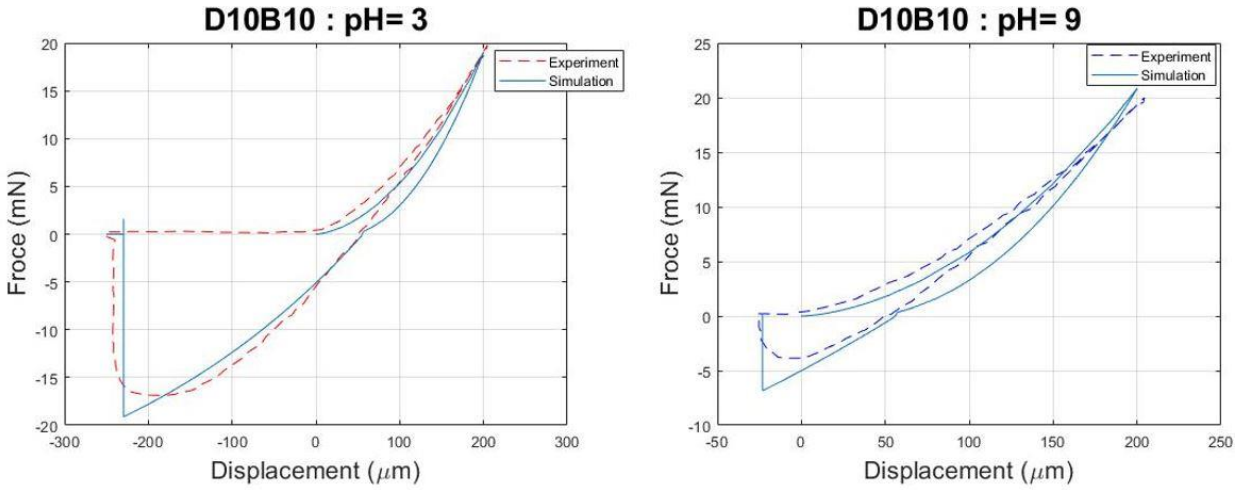

Figure 3.19 : Results of Contact Mechanics Numerical Simulation

Acidic pH Error % = $(|W_{adh}^{m} - W_{adh}^{e}|/W_{adh}^{e})$ X 100 = 7.8649

Basic pH Error % = $(|W_{adh}^{m} - W_{adh}^{e}|/W_{adh}^{e})$ X 100 = 28.3607

Where $W_{adh,}^{m}$ W_{adh}^{e} represent work done by adhesive in simulation, work done by adhesive in experiment respectively. We observe that the simulation can captures the overall trend of material response of adhesive but there is a mismatch between the simulation and experimental results based on the error estimates discussed above. A more advanced bond dissociation kinetics based cohesive law developed in study 2 can be employed to overcome the limitations of the current phenomenological cohesive law. The hyper elastic and viscoelastic parameters calibrated in this study represent the bulk material properties of the adhesive. The parameters governing the traction separation law represent the fracture of interface composed of the bonds at the atomic/molecular formed between the adhesive and substrate at acidic, basic pH. The results of this study can be employed as reference for future simulations to characterize the adhesion of marine mussel based smart adhesives

3.8 Acknowledgement

I would like thank Dr Ameya Narkar and Dr Bruce P Lee for sharing their research conducted on smart adhesives. Based on their numerous experiments conducted on smart adhesives, I was able to characterize the material response and adhesive strength of the polymer by conducted a contact mechanics numerical simulation.

4 Summary

The aim of the first study was to develop an approach based on sensitivity analysis and uncertainty quantification to characterize rate dependent Mode-I Fracture based on a viscoplastic flow cohesive. The first study performed sensitivity analysis to identify K_n , δ_n , δ_f as the most critical factors and uncertainty analysis based on KNN regression model was able to give a reasonably good fit for rate dependent Mode-I fracture experiments for Quasi-static (Strain Rate : 5.08 mm/min) and Dynamic loading (50.8 mm/min & 508 mm/min). This KNN trained model would require further validation by comparing with experiments for rate dependent fracture for a different polymer. Also, a more advanced approach known as "Bayesian Calibration" can be employed to improve the prediction of the present

The second study focused on developing a stochastic bond dissociation kinetics-based traction separation law which is inspired from the evolution of bond probability as function of interfacial separation. The stochastic bonding-based traction separation law can be employed to predict the rate dependent fracture response. The study was able to calculate the input parameters by taking reference from the continuum based cohesive law calibrated for Quasi-static loading developed in study 1. This traction separation was employed to predict Mode-I fracture for different strain rates in reference in study 1. The quasi-static response gave a reasonably good prediction and for higher strain rate, koff had to be updated to improve the prediction. The next stage of this study will be performed uncertainty quantification of the input parameters governing the stochastic bonding cohesive to perform calibration for different polymeric materials

The third study's primary objective was to characterize the material response and adhesion of marine mussel inspired smart adhesives by employing hyper-elastic material model with viscoelasticity and cohesive zone model based on the traction separation in contact mechanics simulation. An arruda boyce material model was able to accurately the hyperelastic material response of adhesive hydrogel and three Maxwell elements with different relaxation modulus and time were able to characterize viscoelastic response. The cohesive zone model employed to characterize adhesive strength assumed mixed mode behavior in Mode -I, II and traction separation parameters were inversely calibrated by comparing with the experimental results. A sensitivity analysis conducted indicated that the fracture in Mode-I is predominant. This result can be employed to reduce the size of the input training data set for calibration for different chemical compositions of smart adhesives. The simulation results demonstrated a need to develop traction separation law based on bond dissociation kinetics to accurately predict the experimental results of the contact mechanics simulation of smart adhesives.

5 Reference List

[1] C. Su, Y. J. Wei, and L. Anand, “An elastic-plastic interface constitutive model: Application to adhesive joints,” *Int. J. Plast.*, 2004, doi: 10.1016/j.ijplas.2003.12.008.

[2] A. Khayer Dastjerdi, E. Tan, and F. Barthelat, “Direct Measurement of the Cohesive Law of Adhesives Using a Rigid Double Cantilever Beam Technique,” *Exp. Mech.*, vol. 53, no. 9, pp. 1763–1772, 2013, doi: 10.1007/s11340-013-9755-0.

[3] M. Elices, G. V Guinea, J. G. Omez, and J. Planas, “The cohesive zone model: advantages, limitations and challenges.” [Online]. Available: www.elsevier.com/locate/engfracmech.

[4] M. D. Banea and L. F. M. Da Silva, “Adhesively bonded joints in composite materials: An overview,” *Proceedings of the Institution of Mechanical Engineers, Part L: Journal of Materials: Design and Applications*, vol. 223, no. 1. pp. 1–18, Jan. 01, 2009, doi: 10.1243/14644207JMDA219.

[5] M. Aniber Benin, B. Stanly Jones Retnam, M. Ramachandran, M. Sivapragash, and J. Edwin Raja Dhas, “Comparative study of tensile properties on thermoplastic & thermosetting polymer composites,” *Int. J. Appl. Eng. Res.*, vol. 10, no. 11, pp. 10109–10113, 2015.

[6] Prof. Dr. Magd Abdel Wahab , “Joining Composites with Adhesives : Theory and Applications”

[7] A. J. Smiley and R. B. Pipes, “Rate Effects on Mode I Interlaminar Fracture Toughness in Composite Materials,” *J. Compos. Mater.*, vol. 21, no. 7, pp. 670–687, 1987, doi: 10.1177/002199838702100706.

[8] E. Panagiotou, K. C. Millett, and P. J. Atzberger, “Topological methods for polymeric materials: Characterizing the relationship between polymer entanglement and viscoelasticity,” *Polymers (Basel).*, vol. 11, no. 3, Mar. 2019, doi: 10.3390/polym11030437.

[9] N. Aurore and J. Julien, “Double cantilever beam tests on a viscoelastic adhesive: Effects of the loading rate,” in *Procedia Structural Integrity*, 2016, vol. 2, pp. 269–276, doi: 10.1016/j.prostr.2016.06.035.

[10] M. R. Sangtabi and M. S. Kiasat, “Long-term viscoelastic properties of an adhesive and molding compound, characterization and modeling,” *Polymer (Guildf).*, vol. 116, pp. 204–217, 2017, doi: 10.1016/j.polymer.2017.03.074.

[11] A. Boyano, J. De Gracia, A. Arrese, and F. Mujika, “Experimental assessment of an End Notched Flexure test configuration with an inserted roller for analyzing

mixed-mode I/II fracture toughness," *Eng. Fract. Mech.*, vol. 163, pp. 462–475, 2016, doi: 10.1016/j.engfracmech.2016.05.012.

[12] R. Gerlach, C. Kettenbeil, and N. Petrinic, "A new split Hopkinson tensile bar design," *Int. J. Impact Eng.*, vol. 50, pp. 63–67, 2012, doi: 10.1016/j.ijimpeng.2012.08.004.

[13] P. Rahulkumar, A. Jagota, S. J. Bennison, and S. Saigal, "Cohesive element modeling of viscoelastic fracture: Application to peel testing of polymers," *Int. J. Solids Struct.*, vol. 37, no. 13, pp. 1873–1897, 2000, doi: 10.1016/S0020-7683(98)00339-4.

[14] B. F. Sørensen and T. K. Jacobsen, "Determination of cohesive laws by the J integral approach," *Eng. Fract. Mech.*, vol. 70, no. 14, pp. 1841–1858, 2003, doi: 10.1016/S0013-7944(03)00127-9.

[15] M. Musto and G. Alfano, "A novel rate-dependent cohesive-zone model combining damage and visco-elasticity," *Comput. Struct.*, vol. 118, pp. 126–133, 2013, doi: 10.1016/j.compstruc.2012.12.020.

[16] N. M. Ames, V. Srivastava, S. A. Chester, and L. Anand, "A thermo-mechanically coupled theory for large deformations of amorphous polymers. Part II: Applications," *Int. J. Plast.*, vol. 25, no. 8, pp. 1495–1539, 2009, doi: 10.1016/j.ijplas.2008.11.005.

[17] C. Xu, T. Siegmund, and K. Ramani, "Rate-dependent crack growth in adhesives: II. Experiments and analysis," *Int. J. Adhes. Adhes.*, 2003, doi: 10.1016/S0143-7496(02)00063-5.

[18] S. Sankararaman and S. Mahadevan, "Integration of model verification, validation, and calibration for uncertainty quantification in engineering systems," *Reliab. Eng. Syst. Saf.*, vol. 138, pp. 194–209, 2015, doi: 10.1016/j.ress.2015.01.023.

[19] M. Lißner, E. Alabort, H. Cui, A. Pellegrino, and N. Petrinic, "On the rate dependent behaviour of epoxy adhesive joints: Experimental characterisation and modelling of mode I failure," *Compos. Struct.*, vol. 189, pp. 286–303, Apr. 2018, doi: 10.1016/j.compstruct.2018.01.019.

[20] C. Xu, T. Siegmund, and K. Ramani, "Rate-dependent crack growth in adhesives: II. Experiments and analysis," *Int. J. Adhes. Adhes.*, vol. 23, no. 1, pp. 15–22, 2003, doi: 10.1016/S0143-7496(02)00063-5.

[21] J. Richeton, S. Ahzi, K. S. Vecchio, F. C. Jiang, and R. R. Adharapurapu, "Influence of temperature and strain rate on the mechanical behavior of three amorphous polymers: Characterization and modeling of the compressive yield stress," *Int. J. Solids Struct.*, vol. 43, no. 7–8, pp. 2318–2335, 2006, doi:

10.1016/j.ijsolstr.2005.06.040.

[22] J. Richeton, S. Ahzi, L. Daridon, and Y. Rémond, “A formulation of the cooperative model for the yield stress of amorphous polymers for a wide range of strain rates and temperatures,” *Polymer (Guildf).*, vol. 46, no. 16, pp. 6035–6043, 2005, doi: 10.1016/j.polymer.2005.05.079.

[23] I. M. Sobol’, “Sensitivity Estimates for Nonlinear Mathematical Models,” 1993.

[24] Y. Song, J. Liang, J. Lu, and X. Zhao, “An efficient instance selection algorithm for k nearest neighbor regression,” *Neurocomputing*, 2017, doi: 10.1016/j.neucom.2017.04.018.

[25] Y. Wei, “A stochastic description on the traction-separation law of an interface with non-covalent bonding,” *J. Mech. Phys. Solids*, vol. 70, no. 1, pp. 227–241, 2014, doi: 10.1016/j.jmps.2014.05.014.

[26] G. I. Bell, “Models for the Specific Adhesion of Cells to Cells Author (s): George I . Bell Published by : American Association for the Advancement of Science Stable URL : https://www.jstor.org/stable/1746930 REFERENCES Linked references are available on JSTOR for t,” vol. 200, no. 4342, pp. 618–627, 2019.

[27] A. R. Narkar, B. Barker, M. Clisch, J. Jiang, and B. P. Lee, “PH Responsive and Oxidation Resistant Wet Adhesive based on Reversible Catechol-Boronate Complexation,” *Chem. Mater.*, vol. 28, no. 15, pp. 5432–5439, 2016, doi: 10.1021/acs.chemmater.6b01851.

[28] A. R. Narkar, “Digital Commons @ Michigan Tech REVERSIBLY SWITCHING ADHESION OF SMART ADHESIVES,” 2018.

[29] P. A. L. S. Martins, R. M. N. Jorge, and A. J. M. Ferreira, “A comparative study of several material models for prediction of hyperelastic properties: Application to silicone-rubber and soft tissues,” *Strain*, vol. 42, no. 3, pp. 135–147, 2006, doi: 10.1111/j.1475-1305.2006.00257.x.

[30] D. MAZURKIEWICZ, “Problems of identification of strength properties of rubber materials for purposes of numerical analysis: a review,” *Arch. Civ. Mech. Eng.*, vol. 10, no. 1, pp. 69–84, 2010, doi: 10.1016/s1644-9665(12)60131-9.

[31] E. M. Arruda and M. C. Boyce, “A three-dimensional constitutive model for the large stretch behavior of rubber elastic materials,” *J. Mech. Phys. Solids*, vol. 41, no. 2, pp. 389–412, 1993, doi: 10.1016/0022-5096(93)90013-6.

[32] T. K. Kim, J. K. Kim, and O. C. Jeong, “Measurement of nonlinear mechanical properties of PDMS elastomer,” *Microelectron. Eng.*, vol. 88, no. 8, pp. 1982–1985, 2011, doi: 10.1016/j.mee.2010.12.108.

[33] F. Cortés and M. J. Elejabarrieta, “Modelling viscoelastic materials whose storage modulus is constant with frequency,” *Int. J. Solids Struct.*, vol. 43, no. 25–26, pp. 7721–7726, 2006, doi: 10.1016/j.ijsolstr.2006.03.022.

[34] B. Babaei, A. Davarian, K. M. Pryse, E. L. Elson, and G. M. Genin, “Efficient and optimized identification of generalized Maxwell viscoelastic relaxation spectra,” *J. Mech. Behav. Biomed. Mater.*, vol. 55, pp. 32–41, 2016, doi: 10.1016/j.jmbbm.2015.10.008.

[35] K. Park and G. H. Paulino, “Cohesive zone models: A critical review of traction-separation relationships across fracture surfaces,” *Appl. Mech. Rev.*, vol. 64, no. 6, 2011, doi: 10.1115/1.4023110.

[36] M. A. Hariri-Ardebili and V. E. Saouma, “Sensitivity and uncertainty quantification of the cohesive crack model,” *Eng. Fract. Mech.*, 2016, doi: 10.1016/j.engfracmech.2016.01.008.

[37] https://upload.wikimedia.org/wikipedia/commons/e/e7/Fracture_modes_v2.svg , Attribution : Twisp / Public domain